Marine Biology (2026) 173:228
https://doi.org/10.1007/s00227-026-04987-3

ORIGINAL PAPER

Climatological assessment of diatom and *Noctiluca scintillans* dynamics in the Arabian Sea

Amit Kumar Jena[1,2] · S. Ayana[3,4] · Susmita Raulo[3,4] · Suchismita Srichandan[5] · Sanjiba Kumar Baliarsingh[3] · Alakes Samanta[3] · T. M. Balakrishnan Nair[3]

Received: 2 June 2026 / Accepted: 23 October 2026
© The Author(s), under exclusive licence to Springer-Verlag GmbH Germany, part of Springer Nature 2026

Abstract

Over the past two decades, the Arabian Sea has witnessed an unprecedented ecological reorganization, characterized by a progressive shift in the composition of winter blooms, with the mixotrophic dinoflagellate Green *Noctiluca scintillans* (GNS) increasingly emerging as a dominant bloom-former alongside, and in some regions replacing, diatoms. In the present study, climatology (2003–2024) of MODIS-Aqua-derived chlorophyll-*a* (chl-*a*), particulate organic carbon (POC), three phytoplankton size classes (micro, nano, and pico), diatom spread area, GNS spread area, sea surface temperature (SST), and surface currents were used to characterize the spatio-temporal evolution of phytoplankton blooms in the Arabian Sea. Results reveal two distinct productivity maxima, a southwest monsoon peak along the upwelling-fringed Somali, Omani, and southwest Indian coasts during July-September, and a northeast monsoon peak in the northern and central Arabian Sea during January-February. Surface chl-*a* and POC reach climatological values exceeding 3 mg m^{-3} and 250 mg m^{-3}, respectively, at peak bloom. Microphytoplankton, dominated by diatoms, contribute the bulk of bloom biomass during both monsoons, whereas picophytoplankton dominate the strongly stratified, oligotrophic spring intermonsoon. Climatological maps reveal that GNS attains its maximum spatial extent during the late winter monsoon (February-March) in the central and northern Arabian Sea, coinciding with diatom decline and the onset of post-mixing stratification. Cooling SST and intensifying northeast monsoon currents precondition the basin for diatom bloom initiation; subsequent silicate depletion may then promote proliferation of GNS. The observed temporal transitions from diatom dominance to GNS proliferation are consistent with the diatom-to-GNS shift hypothesis in the Arabian Sea and highlight the need for further investigation of the underlying mechanisms.

Keywords Phytoplankton size classes · MODIS-aqua · Particulate organic carbon · Bloom · Sea surface temperature

Introduction

The Arabian Sea, occupying the northwestern arm of the north Indian Ocean, is a semi-enclosed, tropical sea that sustains exceptionally high biological productivity comparable to that of temperate continental shelves (Madhupratap et al. 1996). This anomalous productivity arises from the seasonal reversal of the Indian monsoon and the consequent reorganization of upper-ocean physics, which facilitates the nutrient enrichment and nourishes the food chain, sustaining a large fishery (Schott and McCreary 2001; Wiggert et al. 2005; Lotliker et al. 2020; Lakshmi et al. 2021). The basin also hosts one of the world's prominent perennial open-ocean oxygen minimum zones (OMZs) and constitutes a dominant site of pelagic denitrification in the global ocean (Naqvi et al. 2000). The upper few hundred meters of

Responsible Editor: U. Sommer

✉ Sanjiba Kumar Baliarsingh
baliarsingh.s@incois.gov.in

1 Japan Agency for Marine-Earth Science and Technology, Yokohama 236-0001, Kanagawa, Japan

2 Indian Institute of Technology Bombay, Mumbai 400076, Maharashtra, India

3 Indian National Centre for Ocean Information Services, Ministry of Earth Sciences, Government of India, Hyderabad 500090, India

4 Kerala University of Fisheries and Ocean Studies, Kochi 682506, India

5 Department of Marine Sciences, Berhampur University, Bhanja Bihar 760007, Odisha, India

this zone are nearly anoxic and still support animal life, possibly as a result of episodic injections of oxygen by physical processes (Banse et al. 2014). Oxygen concentrations in the intermediate depths of the Arabian Sea are generally suboxic, primarily due to poor ventilation and high biological respiration rates (Lachkar et al. 2019; Sarma et al. 2020). During the southwest monsoon (June-September), the Findlater Jet drives Ekman-divergence-induced upwelling along the Somali, Oman, and southwest Indian coasts, generating the open-ocean blooms in the Indian Ocean (Lee et al. 2000; Kumar et al. 2001; McCreary et al. 2009). During the northeast monsoon (November-February), buoyancy loss from cool, dry continental winds drives convective mixing in the northern basin, entraining nutrients into the euphotic zone (Madhupratap et al. 1996; Retnamma et al. 2021). The intervening intermonsoon periods are characterized by strong stratification, surface nutrient limitation, and oligotrophic conditions dominated by small phytoplankton and an active microbial loop (Garrison et al. 2000; Jyothibabu et al. 2008; Albin et al. 2022).

Within this physically forced framework, phytoplankton size classes (PSCs) provide a biogeochemically meaningful basis for partitioning communities into microphytoplankton (>20 μm), nanophytoplankton (2–20 μm), and picophytoplankton (0.2–2 μm), each occupying distinct ecological and biogeochemical niches (Sieburth et al. 1978). Microphytoplankton, dominated by diatoms, characterize nutrient-replete turbulent waters and enhance the biological carbon pump (Smetacek 1999). Nanophytoplankton dominate mesotrophic transitional regimes, whereas picophytoplankton, comprising prokaryotic cyanobacteria such as Prochlorococcus and Synechococcus, dominate stratified oligotrophic waters where regenerated production prevails (Hirata et al. 2011; Karnan et al. 2017; Albin et al. 2022). The strong relationship between size and phytoplankton function has led to a variety of bio-optical models that are designed for use in remote sensing to map PSCs on global and regional scales (Ciotti and Bricaud 2006; Devred et al. 2006; Uitz et al. 2006; Hirata et al. 2008). Several abundance-based and semi-analytical satellite algorithms now permit the retrieval of PSCs from ocean colour data (Brewin et al. 2010; Sahay et al. 2017), enabling basin-scale assessments of community structure that are unattainable through sparse in situ pigment sampling alone.

Historically, diatoms have dominated Arabian Sea monsoon blooms (Tarran et al. 1999; Garrison et al. 2000), reflecting their high maximum growth rates, large nutrient storage vacuoles, and tendency to form rapidly sinking aggregates that efficiently transfer carbon and biogenic silica to depth (Smetacek 1999). However, diatom dominance is contingent upon adequate silicate supply; once Si: N ratios decline, non-siliceous phytoplankton can outcompete them (Egge and Aksnes 1992; Lakshmi et al. 2021; Goldenberg et al. 2022; Shetye et al. 2023). Against this backdrop, the recent emergence of green *Noctiluca scintillans* (hereafter GNS) as the dominant winter bloom-former in the central and northern basin represents one of the most striking ecological reorganizations in any major open-ocean ecosystem in recent decades (Gomes et al. 2014; Lotliker et al. 2018). Unlike most dinoflagellates, the GNS harbours an obligate prasinophyte symbiont, *Pedinomonas noctilucae*, exhibits a mixotrophic lifestyle, and is well-adapted to tropical waters. This form is largely reported from regions across the Indian Ocean and the tropical Pacific (Sweeney 1971; Hansen et al. 2004; Furuya et al. 2006; Stoecker et al. 2017; Liu et al. 2025; Manigandan et al. 2024). The GNS bloom does not produce toxins, but its dense aggregations can create hypoxic conditions and increase the ammonium concentrations in the water column, which can initiate significant mortality in fish and invertebrate communities (Zahir et al. 2023; Nayak et al. 2025).

This diatom-to-GNS shift carries significant biogeochemical and trophic consequences (Gomes et al. 2014). Diatoms support short, energy-efficient grazing pathways from primary producers to fish through copepods and drive efficient export of particulate organic carbon (POC) (Cushing 1989; Tréguer et al. 2018). In contrast, GNS is a poor prey resource for traditional copepods because of its size, gelatinous body, and ammonium-rich cytoplasm, with only specialist consumers exploiting it (Padmakumar et al. 2012; Matondkar et al. 2012). Owing to their mixotrophic nutritional strategy, they can consume fish and copepod eggs, as well as other coexisting phytoplankton species, potentially leading to ecological imbalance (He et al. 2021; Bharathi et al. 2023; Manigandan et al. 2024). Bloom collapse leads to mass settling of moribund cells whose decomposition stimulates further oxygen demand, potentially reinforcing hypoxia through positive feedback (Naqvi et al. 2000; Gomes et al. 2014). Replacement of diatoms by GNS therefore weakens carbon export, alters energy flow through the food web, and threatens regional fisheries on which millions of people depend (Tréguer et al. 2018). In India, both historical and recent reports indicate that bloom-associated fish kills are mainly caused by dinoflagellates, particularly GNS (Raj et al. 2020; Samanta et al. 2023; Mariasingarayan et al. 2025). Satellite-derived POC further provides an integrative measure of upper-ocean carbon stocks (Stramski et al. 2008; Shahimol et al. 2025); its joint analysis with chlorophyll-*a* (chl-*a*) and PSCs reveals the partitioning of biogenic carbon between living and detrital pools, as well as the temporal phasing of bloom development and termination.

Despite extensive prior research, an integrated, basin-wide climatological synthesis that simultaneously resolves total chl-*a*, the three PSCs, diatoms, GNS, POC, sea surface

temperature (SST), and surface currents on a single consistent MODIS-Aqua monthly grid remains scarce. Such a synthesis is essential as a baseline against which to evaluate interannual anomalies, climate-driven changes, and the ongoing diatom–GNS trajectory. Accordingly, the present study aims to (i) document the climatological monthly evolution of total chl-*a* and the three PSCs in the Arabian Sea using MODIS-Aqua observations; (ii) characterize the spatio-temporal dynamics of diatoms and GNS within this size-structured framework; (iii) examine the covariation of POC with chl-*a* and PSCs to interpret bloom development and detrital carbon pools; (iv) link observed biological patterns to physical forcing through climatological SST and surface currents; and (v) discuss mechanisms underlying the diatom–GNS shift and its implications for biogeochemistry and ecosystem functioning. The analysis is intended both as a comprehensive descriptive baseline of the modern Arabian Sea ecosystem and as an interpretive framework for understanding ongoing and projected change.

Materials and methods

Study area

The study area encompasses the entire Arabian Sea, broadly defined here as the region bounded by approximately 5°-27°N and 45°-78°E (Fig. 1). The basin is bordered to the west by the Horn of Africa and the Arabian Peninsula, to the north by Iran and Pakistan, to the east by the western coast of India, and to the south it merges with the equatorial Indian Ocean. The northern Arabian Sea comprises deep ocean basins, with the Carlsberg Ridge separating the eastern (Arabian) and western (Somali) basins. Two productive marginal seas, the Persian Gulf and the Red Sea, exchange dense, saline outflows with the Arabian Sea through the Strait of Hormuz and the Bab-el-Mandeb, respectively. The basin is influenced by the seasonally reversing monsoon wind system: southwesterly winds prevail during boreal summer (June-September), generating a strong cross-equatorial flow, and the Findlater Jet, and northeasterly winds prevail during boreal winter (November-February) (Schott and McCreary 2001). The Arabian Sea exhibits seasonally distinct productivity patterns, with peak productivity occurring in the western and southeastern region during the summer monsoon and in the northern region during winter. In contrast, inter-monsoon periods are generally oligotrophic (Thoppil 2023). Monsoon-driven changes in mixed-layer depth, thermocline position, and coastal upwelling enhance nutrient supply and support high phytoplankton biomass and productivity (Goes et al. 2005; Khan et al. 2023; Wiggert et al. 2005; Kumar et al. 2010). These wind regimes drive corresponding reversals in the surface circulation: clockwise in summer (the Somali Current flowing northward, the West Indian Coastal Current flowing southward) and anticlockwise in winter (the Somali Current reversing southward, the West Indian Coastal Current flowing northward).

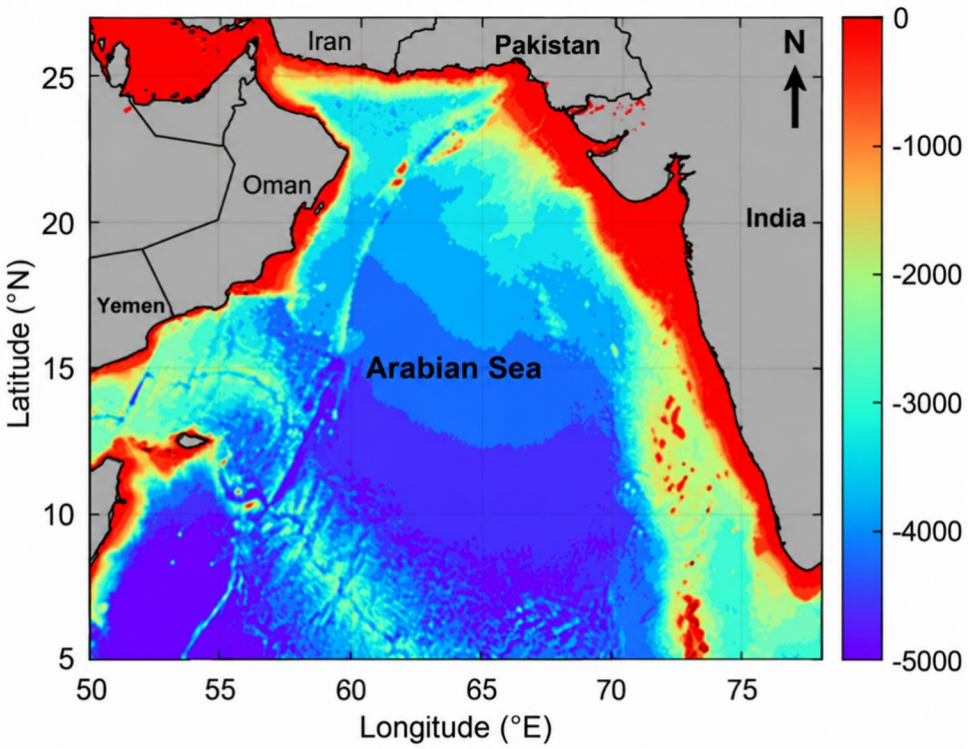


Fig. 1 Study area in the Arabian Sea showing the spatial extent of the analysis region and its location relative to the surrounding coastal countries. The spatial distribution of seafloor bathymetry (in metres) is represented by the colour scale, with depths ranging from 0 m (red) to approximately − 5000 m (purple)

MODIS-Aqua-derived chlorophyll-*a* and POC

Level-3 monthly composite ocean colour products from the Moderate Resolution Imaging Spectroradiometer aboard the Aqua satellite (MODIS-Aqua), spanning the period January 2003 to December 2024 (22 years), were obtained from the NASA Ocean Biology Distributed Active Archive Center (OB.DAAC; https://oceancolor.gsfc.nasa.gov). Surface chl-*a* (mg m^{-3}) was retrieved using the standard sensor-default bio-optical algorithm (O'Reilly et al. 1998). POC (in mg m^{-3}) was retrieved using the empirical blue-to-green reflectance ratio algorithm of Stramski et al. (2008), which has been globally validated against in situ POC concentrations and is the operational MODIS-Aqua POC product. Both chl-*a* and POC were processed at a nominal spatial resolution of 4 km and re-binned.

Phytoplankton size classes

Three PSC fractions of total chl-*a* were derived following the abundance-based, three-component model of Sahay et al. (2017), which is itself an Arabian Sea-specific recalibration of the framework originally proposed by Sathyendranath et al. (2004) and refined by Brewin et al. (2010, 2015). The model partitions total surface chl-*a* (C) into contributions from microphytoplankton (>20 µm; C_m), nanophytoplankton (2–20 µm; C_n), and picophytoplankton (<2 µm; C_p), such that $C = C_m + C_n + C_p$. Regional parameterization was performed by Sahay et al. (2017) on a pooled in situ dataset comprising shipboard size-fractionated chl-*a* measurements together with phytoplankton pigment data. This regional formulation is consistent with the global models (Hirata et al. 2008). Validation against independent in situ stations confirmed the superiority of the regional tuning over the original Indian Ocean parameterization. For application to satellite observations, the model was driven by Level-3 chl-*a* fields from MODIS-Aqua (4 km) obtained from the NASA Ocean Color Web (https://oceancolor.gsfc.nasa.gov). To represent PSC dominance independently of the overall biomass level, the relative percentage contribution of each size class to total chl-*a* was computed for every climatological month as Cm/C, Cn/C, and Cp/C, expressed as a percentage. The resulting monthly maps of fractional contribution are provided in the Supplementary Material (Supplementary Fig. 1a, b).

Diatom and *Noctiluca scintillans* occurrence

To resolve the species-level structure of the mixed winter bloom of the Arabian Sea, the spectral discrimination algorithm developed by Dwivedi et al. (2015) was applied to MODIS-Aqua imagery. This algorithm exploits the species-specific shape of the remote sensing reflectance spectrum (R_{rs}) to separate four optically distinct water classes: GNS, diatoms, non-bloom oceanic waters, and non-bloom coastal waters. Its development rests on hyperspectral R_{rs} measurements (350–800 nm at 1 nm resolution) acquired with a Satlantic free-fall profiling radiometer during several expeditions in the Arabian Sea, complemented by concurrent microscopic enumeration of cell abundances for both target taxa.

The algorithm's optical rationale is based on the unique pigment and morphological signature of GNS in the Arabian Sea. R_{rs} spectra of GNS-dominated waters exhibit a characteristic monotonic increase from 440 to 550 nm, peaking near 550 nm, a feature absent in diatom-dominated and non-bloom waters. This pattern is attributable to the combined effect of enhanced backscattering by the large, vacuolated GNS cells and pigment absorption by the bioluminescent emission of the dinoflagellate between 420 and 580 nm and to the spectral influence of its prasinophyte endosymbiont *Pedinomonas noctilucae* (Balch and Haxo 1984; Dwivedi et al. 2015). In contrast, diatom spectra are comparatively flat across 440–550 nm. To translate these qualitative differences into a classification rule, the first derivative of R_{rs} with respect to wavelength was computed from MODIS-Aqua bands. The spectral derivative at 488 nm provided maximal class separability and was retained because retrieval uncertainty in R_{rs} increases at longer wavelengths. GNS yielded large positive derivative values at 488 nm, diatoms produced small values straddling zero, and non-bloom oceanic pixels generated large negative values. Class boundaries were further reinforced in a two-dimensional feature space defined by $R_{rs}(488) - R_{rs}(443)$ and $R_{rs}(488) - R_{rs}(531)$, within which the four water types occupied distinct, non-overlapping clusters. The resulting thresholds were applied pixel-by-pixel to MODIS-Aqua Level-3 R_{rs} products at 443, 488, and 531 nm, processed in SeaDAS (Dwivedi et al. 2015). Subsequent independent assessments using shipboard microscopy and Biogeochemical-Argo profiles have reported detection accuracies of 76% for GNS and 92% for diatoms (Lotliker et al. 2018), and the same algorithm has since been adopted in studies of bloom phenology (Baliarsingh et al. 2018; Lotliker et al. 2020).

Sea surface temperature, sea level anomaly and sea surface currents

Monthly composite SST (°C) was obtained from the MODIS-Aqua thermal-infrared Level-3 SST product (4 km, OB.DAAC). Surface current fields (zonal u and meridional v components, cm s^{-1}) were obtained from the Ocean Surface Current Analyses Real-time (OSCAR) Third-Degree resolution product (Bonjean and Lagerloef 2002), which

combines satellite altimetry-derived geostrophic currents with scatterometer-derived Ekman currents. OSCAR currents represent the average surface flow in the upper ~ 30 m of the water column and have been widely used in monsoonal Indian Ocean studies (Schott and McCreary 2001; McCreary et al. 2009). Speed was computed as the magnitude of the velocity vector ($\sqrt{(u^2 + v^2)}$). Daily gridded Level-4 Sea Level Anomaly (SLA) data, with a spatial resolution of ~ 25 km, along with the corresponding geostrophic current components, were obtained from the Copernicus Marine Environment Monitoring Service (https://marine.copernicus.eu).

Climatology and analysis

All datasets were temporally aggregated into monthly climatologies covering the overlapping common period 2003–2024 (22 years). For each calendar month, all available daily or weekly composites were averaged pixel-wise, after quality flagging and removal of glint-, cloud-, and stray-light-affected pixels. The resulting twelve monthly climatologies were used to construct the spatio-temporal evolution maps shown in Figs. 2, 3, 4, 5, 6, 7, 8, 9, 10 and 11. Visual inspection of the climatologies, for sub-regions of the basin (the Somali upwelling zone, the Omani upwelling zone, the central Arabian Sea, and the eastern Arabian Sea/southwest Indian shelf), formed the basis of the descriptive and interpretive analysis presented below. Where appropriate, observed patterns are compared with published in situ and modelling results to corroborate or contextualise the satellite signal.

Uncertainties and limitations of the satellite retrievals

The satellite products employed here carry retrieval uncertainties that warrant explicit acknowledgement. Surface chl-*a* is an optical proxy for phytoplankton biomass rather than a direct measure of cell abundance or growth, and the carbon-to-chlorophyll ratio varies with taxonomic composition, photoacclimation, and nutrient status (Sathyendranath et al. 2009). Consequently, a given chl-*a* concentration need not correspond to a fixed phytoplankton abundance or community structure, and comparable chl-*a* values may arise from optically distinct assemblages. The abundance-based PSC model of Sahay et al. (2017) infers size structure from total chl-*a* through empirically constrained relationships between biomass and the fractional contribution of each size class; because these relationships are statistical, the model reproduces the mean tendency for large cells to dominate

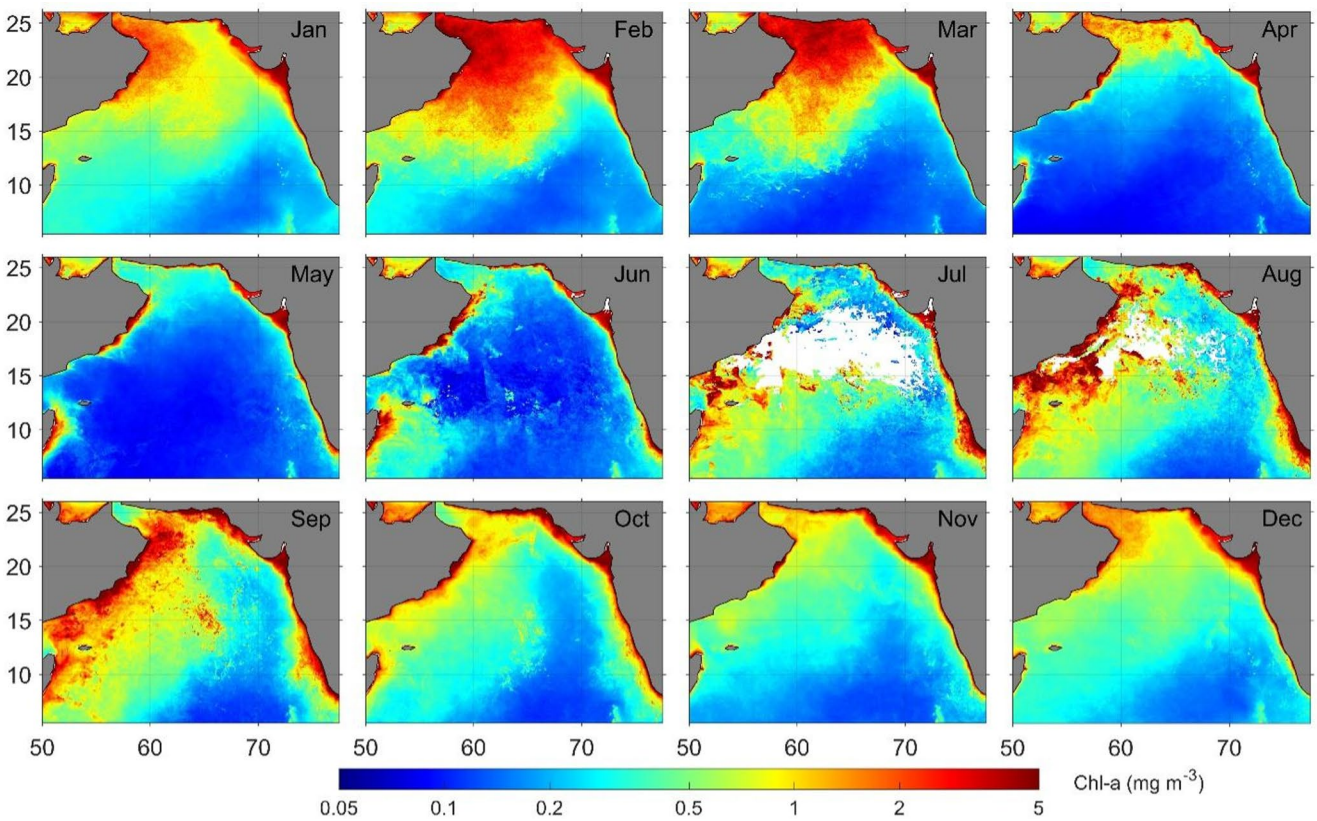


Fig. 2 Monthly climatological distribution of surface chlorophyll-*a* (chl-*a*; mg m^{-3}) in the Arabian Sea, illustrating the seasonal evolution of phytoplankton biomass from January to December. The x-axis represents longitude (°E), and the y-axis represents latitude (°N)

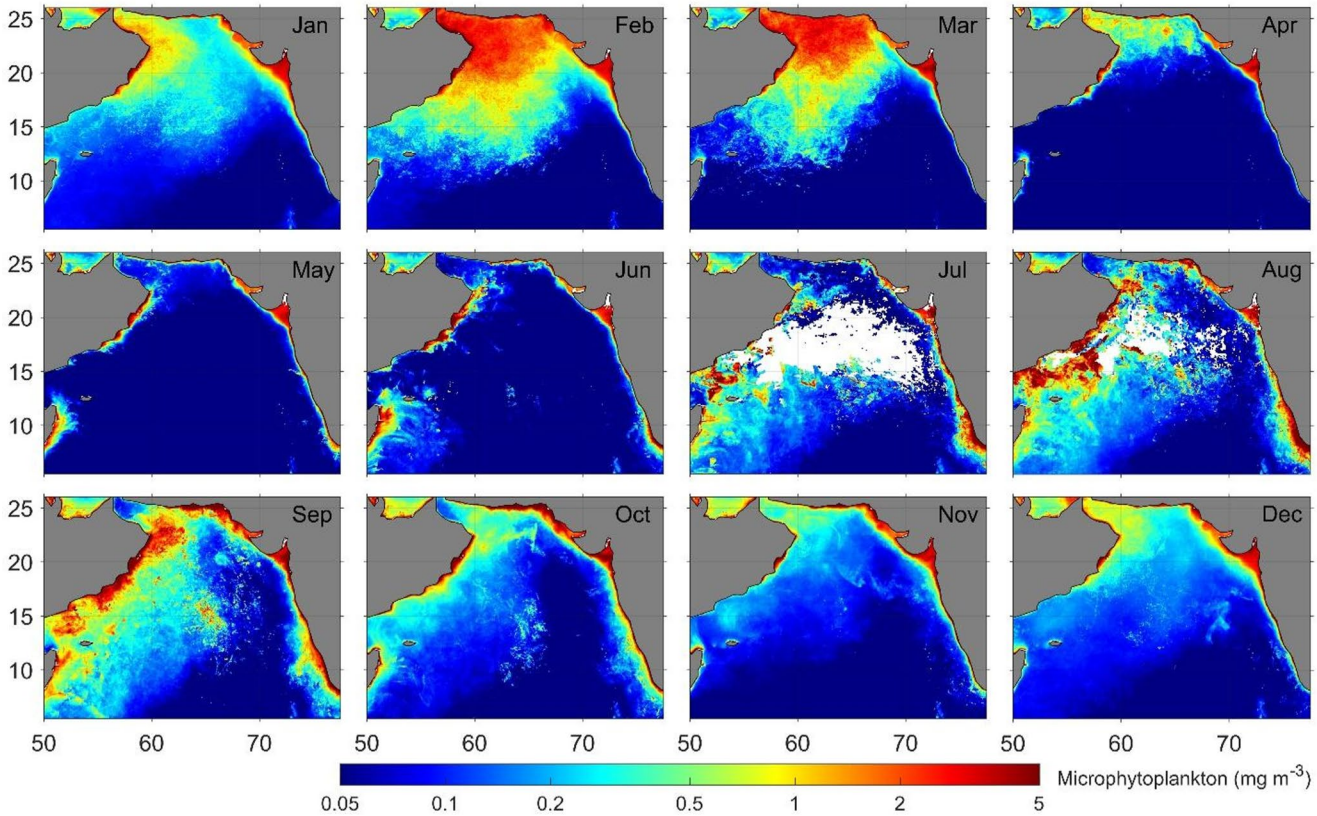


Fig. 3 Monthly climatology of surface microphytoplankton biomass (mg m^{-3}) in the Arabian Sea, showing its spatial distribution and seasonal evolution throughout the annual cycle. The x-axis represents longitude (°E), and the y-axis represents latitude (°N)

at high biomass but cannot resolve community shifts that occur at approximately constant chl-*a*, such as the replacement of one taxon by another of comparable biomass under changing nutrient regimes (Brewin et al. 2010, 2011). Intercomparison studies further indicate that abundance-based retrievals tend to overestimate the picophytoplankton fraction and to underestimate the nanophytoplankton fraction in transitional and mesotrophic waters, where the assumptions of the underlying biomass-size relationship are least well-satisfied (Brewin et al. 2011; Hirata et al. 2011). The diatom and GNS discrimination of Dwivedi et al. (2015) is likewise a reflectance-based classification whose reported detection accuracies of 92% for diatoms and 76% for GNS (Lotliker et al. 2018) imply a non-trivial rate of misclassification, particularly in optically complex coastal waters and under conditions of overlapping or mixed blooms. Moreover, nutrient enrichment can promote opportunistic phytoplankton groups whose contribution to community structure is not fully captured by chl-*a*-based products. These limitations do not compromise the basin-scale climatological patterns described below, which are robust to pixel-level uncertainty by virtue of multi-year monthly averaging, but they caution against over-interpreting absolute fractional values or short-lived features and underscore the value of complementary in situ observations.

Results and Discussion

Climatological evolution of total chlorophyll-*a*

The monthly climatology of total chl-*a* (Fig. 2) reveals two distinct periods of elevated surface biomass separated by two periods of oligotrophy, in clear correspondence with the alternating monsoon and intermonsoon regimes. During the southwest monsoon (June- September), chl-*a* values exceed 3 mg m^{-3} along a continuous belt encompassing the Horn of Africa, the southern Arabian Peninsula, and the southwest Indian shelf, with peak basin-wide concentrations attained in July-August. The spatial structure of this bloom belt closely mirrors the Findlater Jet axis and the locations of well-documented coastal upwelling cells off Cape Guardafui, Ras al Hadd, and the southwest Indian coast (Lee et al. 2000; Kumar et al. 2001; Lévy et al. 2007). The bloom front extends offshore as large filaments and cold-water plumes, whose offshore propagation is consistent with eddy-driven advection in the western boundary regime. The interior of

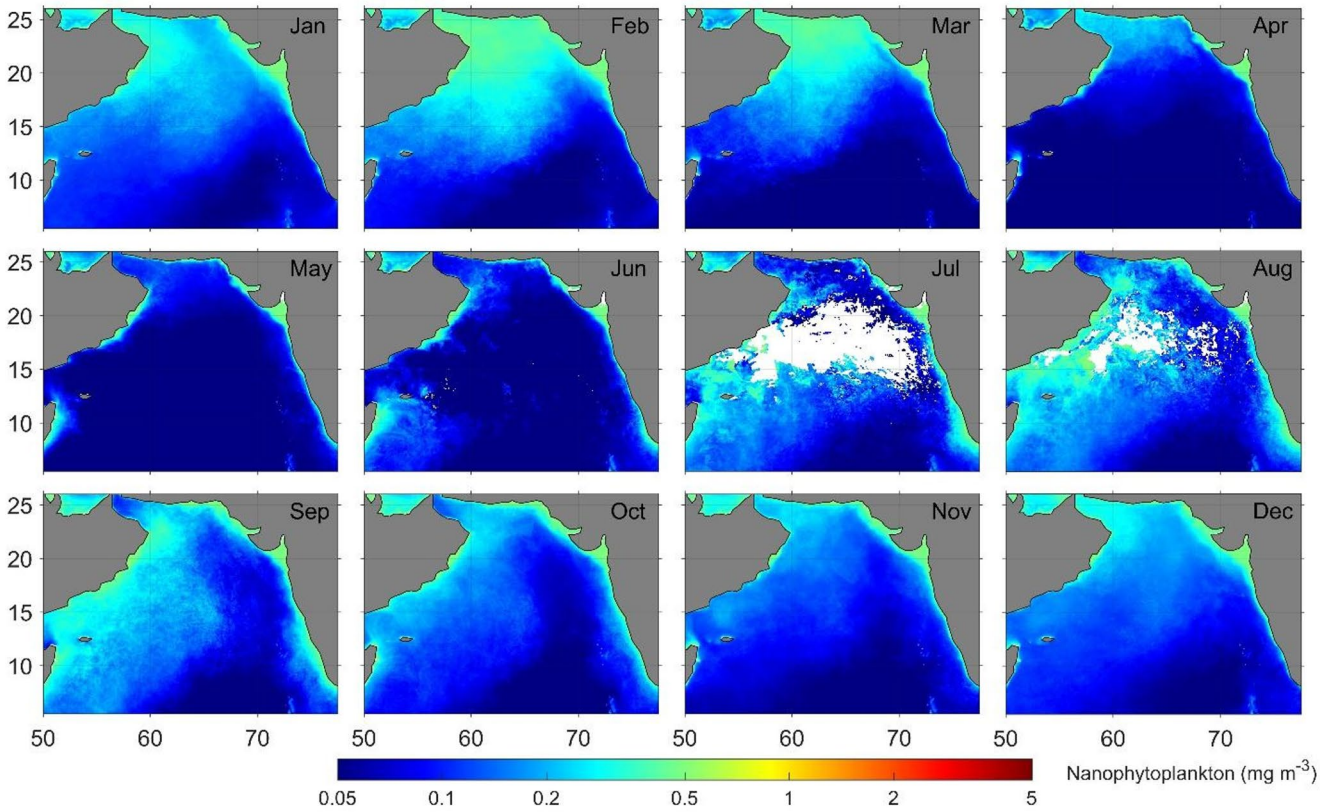


Fig. 4 Monthly climatology of surface nanophytoplankton biomass (mg m^{-3}) in the Arabian Sea, showing its spatial distribution and seasonal evolution throughout the annual cycle. The x-axis represents longitude (°E), and the y-axis represents latitude (°N)

the basin remains comparatively low in chl-*a* (~0.2–0.5 mg m^{-3}) during the southwest monsoon, indicating that primary production at this time is concentrated near the western and eastern boundaries.

A second basin-wide chl-*a* maximum is observed during the northeast monsoon (December-February), when surface concentrations of 0.5–1.5 mg m^{-3} cover the entire northern and central Arabian Sea, with the highest values (>2 mg m^{-3}) appearing in the northern interior (north of ~18°N) in January-February. This convectively-driven open-ocean bloom is the signature of the well-described 'inverse' productivity regime of the northern Arabian Sea, in which dry, cool continental winds force buoyancy loss, deepening of the mixed layer, and entrainment of nutrients into the euphotic zone (Madhupratap et al. 1996; Banse 1987; Lakshmi et al. 2021). Unlike the southwest monsoon bloom, which is laterally constrained to coastal upwelling regions, the northeast monsoon bloom is genuinely open-ocean feature of the northern and central basin and reflects a uniformly applied buoyancy forcing.

Between these two productive periods, the spring intermonsoon (March-May) is characterized by very low surface chl-*a* (often < 0.15 mg m^{-3}) across most of the basin, indicative of strong stratification, nutrient limitation in the surface layer, and ascendancy of small phytoplankton supported by a regenerated production regime. A weaker oligotrophic interval recurs during the brief fall intermonsoon (October-November) before the onset of northeast monsoon convection. The clear bimodal seasonality, observed consistently in the climatology, is unique among the world's oceans and is the direct biological imprint of the reversing monsoon wind system.

Phytoplankton size class structure

The total chl-*a* signal decomposed into informative contributions from the three operational PSCs. The monthly relative contributions of the three size classes to total chl-*a* are mapped in Supplementary Fig. 1 (a, b) and reveal pronounced seasonal and regional shifts in PSC dominance. Microphytoplankton (Fig. 3) closely tracks the spatial and temporal distribution of total chl-*a*, with strong dominance during the southwest-monsoon coastal upwelling bloom and the northeast-monsoon convective bloom. During July-August, microphytoplankton constitute > 60–70% of total chl-*a* along the Somali, Omani, and southwest Indian shelf upwelling zones, and during January-February they exceed 50% of total chl-*a* across the convectively-mixed northern

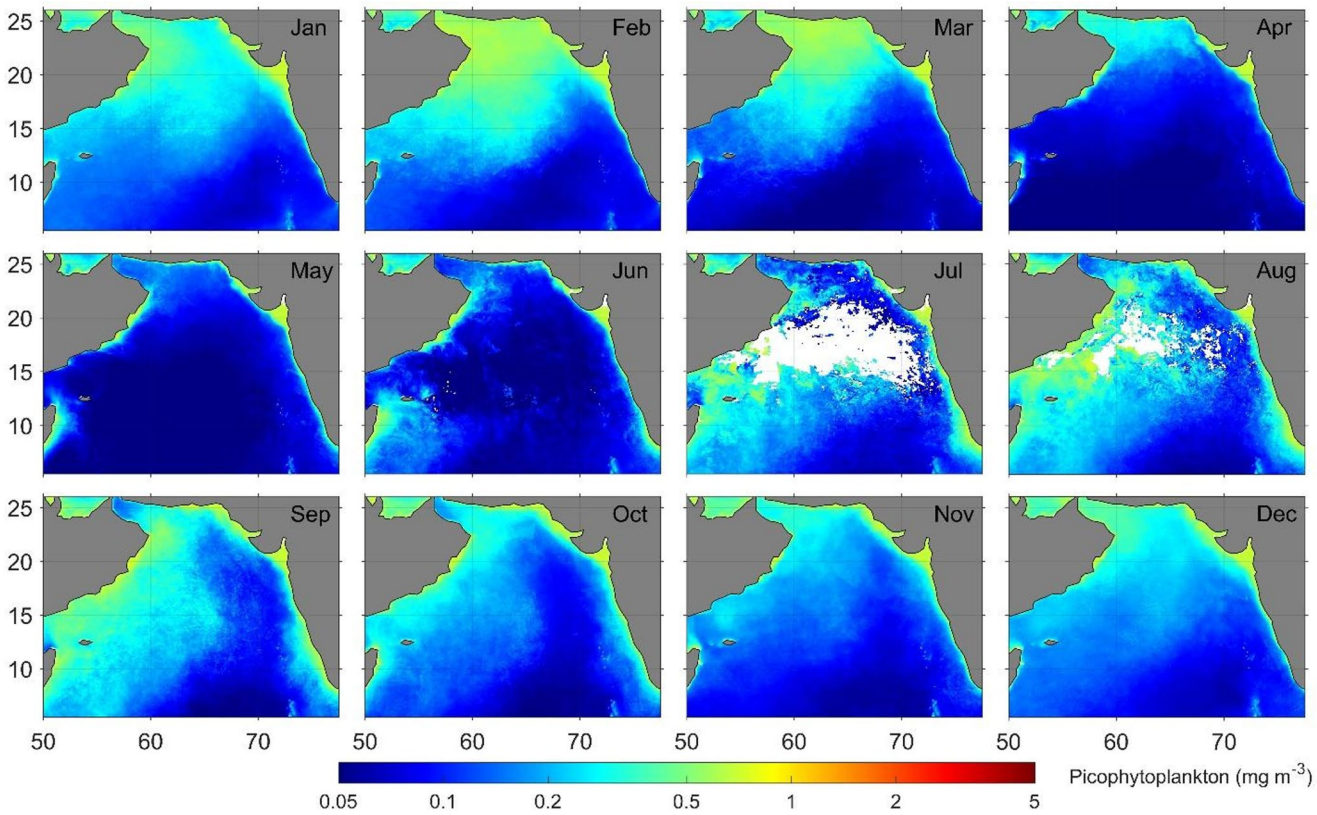


Fig. 5 Monthly climatology of surface picophytoplankton biomass (mg m^{-3}) in the Arabian Sea, showing its spatial distribution and seasonal evolution throughout the annual cycle. The x-axis represents longitude (°E), and the y-axis represents latitude (°N)

interior (Supplementary Fig. 1). These observations are fully consistent with the global pattern of microphytoplankton dominance under nutrient-rich, well-mixed conditions, and with the empirical, abundance-based size-chl-*a* relationship that underpins the Sahay et al. (2017) algorithm. They are also corroborated by extensive in-situ pigment and microscopy data from the Joint Global Ocean Flux Study (JGOFS) Arabian Sea Process Study, which documented diatom-dominated microphytoplankton communities during both monsoons (Tarran et al. 1999; Garrison et al. 2000; Latasa and Bidigare 1998).

Nanophytoplankton (Fig. 4) display a more attenuated seasonality. Their relative contribution is highest during the transition months between bloom and oligotrophic regimes (May-June at the onset of the southwest-monsoon and October-November at the onset of the northeast-monsoon), where they account for 30–45% of total chl-*a* in mesotrophic waters (Supplementary Fig. 1). This pattern is systematically interpretable: nanophytoplankton, which include flagellates, small diatoms and coccolithophores, occupy an intermediate ecological niche between diatoms and picophytoplankton, thriving where nutrients are sufficient to sustain growth above the picophytoplankton-dominant equilibrium but where turbulence and nutrient supply are insufficient to permit the runaway proliferation of large diatoms (Brewin et al. 2010; Hirata et al. 2011). Notably, in the central and eastern Arabian Sea during the late winter monsoon (February-March), nanophytoplankton remain a substantial component (~25–35% of total chl-*a*) even as microphytoplankton concentrations decline, suggesting a transitional community structure during the post-bloom decay of the northeast-monsoon bloom (Supplementary Fig. 1).

Picophytoplankton (Fig. 5) exhibit the inverse seasonality of microphytoplankton, attaining their highest relative dominance (>60% of total chl-*a*) during the spring intermonsoon (March-May) when the basin is strongly stratified and oligotrophic (Supplementary Fig. 1). The southern Arabian Sea, equatorward of approximately 10 °N, sustains high picophytoplankton dominance throughout much of the year, reflecting its persistent thermal stratification, weak vertical nutrient supply and proximity to oligotrophic gyre regimes typical of low-latitude oceans. Absolute picophytoplankton chl-*a* varies less seasonally than the larger size classes, in line with the well-established observation that picophytoplankton biomass is buffered around relatively stable values across nutrient regimes, with bloom episodes contributing primarily through addition of larger cells rather than through expansion of picophytoplankton (Hirata et

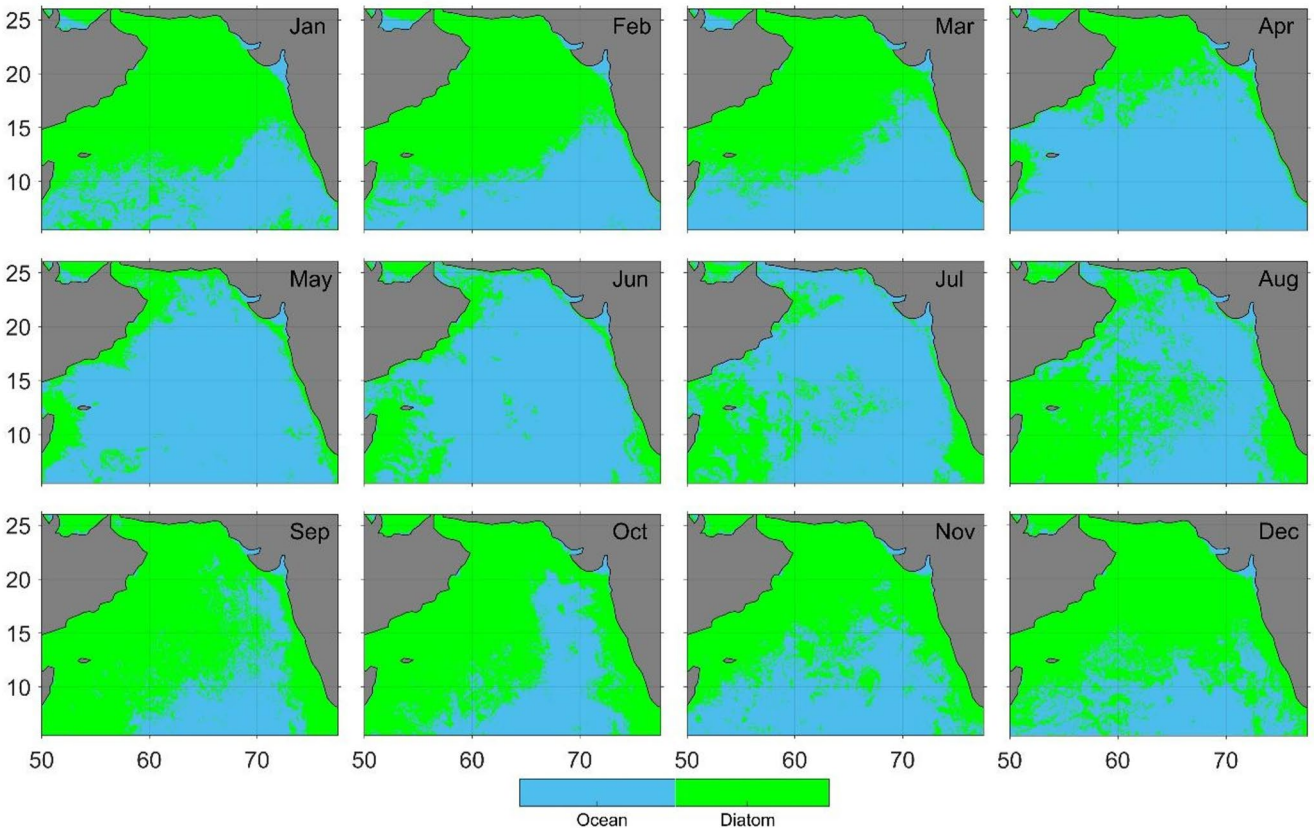


Fig. 6 Monthly climatology of the satellite-retrieved spatial distribution of diatom spread area in the Arabian Sea, illustrating seasonal changes in phytoplankton community composition throughout the annual cycle. The x-axis represents longitude (°E), and the y-axis represents latitude (°N). The legend distinguishes between diatoms (green) spread area pixels and the oceanic (blue) pixels

al. 2011; Falkowski and Woodhead 1992). This buffered behaviour is biogeochemically significant, it means that the additional carbon fixation associated with monsoonal blooms is overwhelmingly channelled through large cells, thereby enhancing the biological carbon pump.

The PSC transitions described above are ultimately governed by the seasonal supply and stoichiometry of macronutrients, for which the Arabian Sea is well characterized by in situ and modelling studies, even though basin-wide satellite nutrient fields are unavailable. During the southwest monsoon, coastal upwelling along the Somali and Omani margins raises surface nitrate to values that frequently exceed several μmol L^{-1}, with commensurate increases in silicate and phosphate that sustain the diatom-dominated microphytoplankton bloom (Morrison et al. 1998; Kumar et al. 2000). In general, larger phytoplankton are favoured by wind-driven coastal upwelling and offshore Ekman pumping, which elevate the nutrient concentration in the euphotic zone. Previous studies have reported that during southwest monsoon upwelling along the eastern Arabian Sea shelf, the combined micro and mesophytoplankton fraction contributes, or up to ~66% of total chl-*a* or ~43 mg chl-*a* m^{-2} (Albin et al. 2022). During the peak summer monsoon upwelling in 2018, shoaling of the nutriclines and a relatively high mixed-layer N: P ratio (8.4±5.25) substantially enhanced phytoplankton biomass in the southern coastal eastern Arabian Sea, where vertically integrated chl-*a* reached 129±96 mg m^{-2} (Reddy et al. 2024). The same study has shown diatoms comprising as much as 65% of the phytoplankton biomass in the central eastern Arabian Sea, while they only made up ~22–33% in the southern and northern sectors, which were weakly upwelled. The nutricline deepened, and mixed-layer N: P ratios decreased to 3.33±2.77 in coastal waters and 3.35±2.26 offshore as upwelling reduced during the late summer monsoon (Reddy et al. 2024). In August 2017 and 2018, a complementary transect along 64°E showed that microphytoplankton contributed about 50% in the northern part of the central Arabian Sea through upwelling and advective enrichment of nutrients, whereas picophytoplankton contributed over 50% in the warmer, nutrient-deficient southern region; the contribution of nanophytoplankton remained relatively constant at 20–30% (Chowdhury et al. 2024).

During the northeast monsoon, convective entrainment resupplies nitrate to the euphotic zone of the northern and central basin, whereas the intermonsoon periods are marked

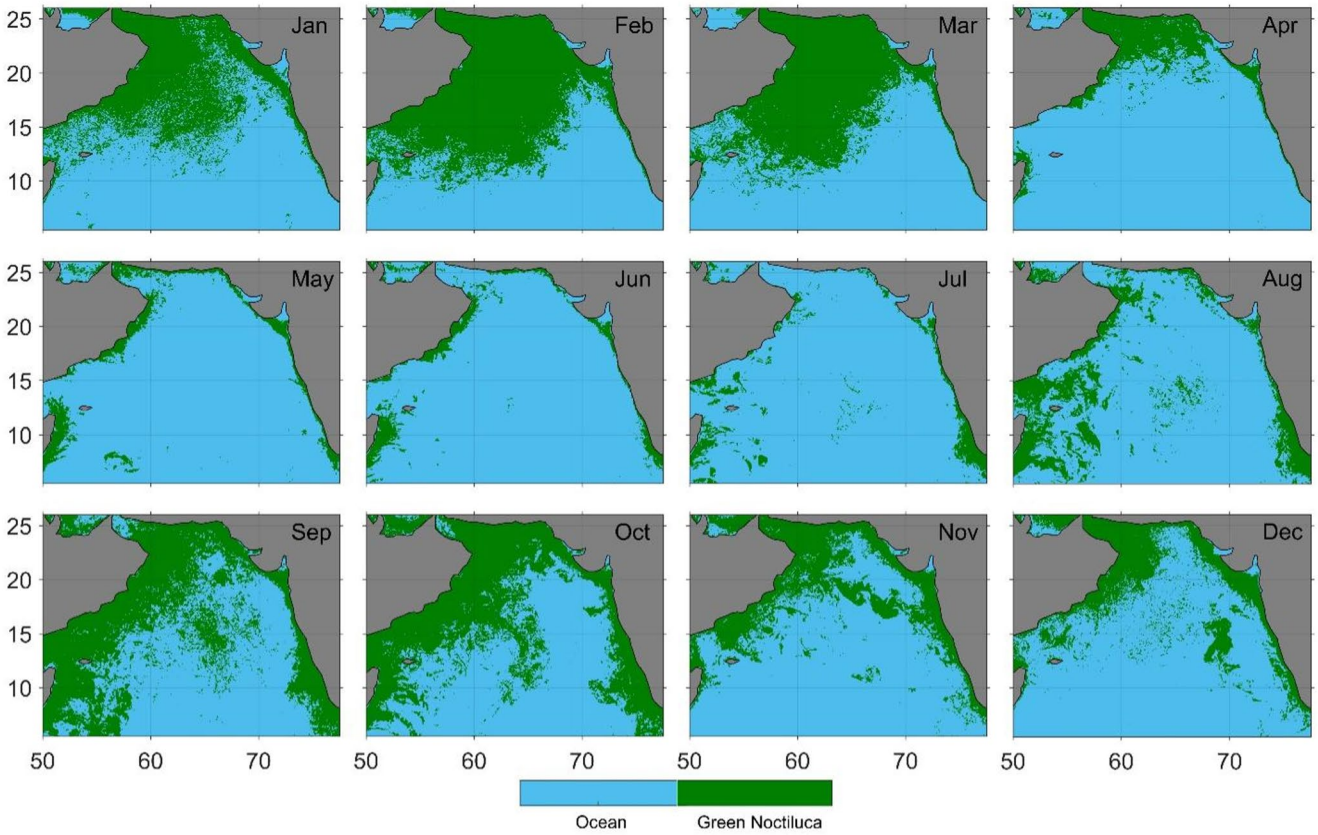


Fig. 7 Monthly climatology of the spatial distribution of green *Noctiluca scintillans* spread area in the Arabian Sea, illustrating its seasonal occurrence and basin-scale variability throughout the annual cycle. The x-axis represents longitude (°E), and the y-axis represents latitude (°N)

by surface nutrient depletion and a shift toward regenerated production and picophytoplankton dominance (Wiggert et al. 2005; Koné et al. 2009). Critically, newly supplied Arabian Sea water carries Si: N ratios near or below unity (Morrison et al. 1998), so that silicate is exhausted before nitrate as blooms progress; the resulting silicate limitation is the proximate nutrient control that terminates diatom growth and opens the niche subsequently occupied by non-siliceous and mixotrophic taxa (Koné et al. 2009). Deeper mixing does not always result in a large-celled phytoplankton bloom. The northern Arabian Sea showed mixed-layer depths greater than 100 m, the uppermost layer nitrate and silicate concentrations of about 2.5 µmol L^{-1} each, phosphate concentrations of 1–2 µmol L^{-1}, and integrated nitrate inventories of about 200–300 mmol m^{-2} during the 2019 winter monsoon, but surface chl-*a* was only 0.1–0.3 µg L^{-1}. This lower productivity response corresponded to a deep mixed layer below the euphotic zone and a Si: DIN ratio less than one, which subsequently imposed light limitations on the phytoplankton community and silicate stress on diatoms (Lakshmi et al. 2021). Thus, silicate exhaustion should be regarded as a seasonally and regionally specific control when Si: DIN is less than one, especially in areas where the silicicline is below the nitracline. In such areas, diatom production might be selectively restricted while nitrate and phosphate continue to be available, thereby favouring non-siliceous, pico-sized, or mixotrophic taxa such as GNS.

Superimposing this nutrient framework on the PSC climatology complements the observed sequence of microphytoplankton dominance under nutrient-replete mixing, nanophytoplankton prevalence in transitional mesotrophic waters, and picophytoplankton dominance under oligotrophic stratification, and it provides the biogeochemical context needed to interpret the spatio-temporal variability in PSC and productivity. The seasonal PSC pattern can also be altered by the influence of interannual variations in monsoon intensity. During the weakened southwest monsoon associated with the 2015–2016 El Niño event, microphytoplankton contributed about 23% of total chl-*a*, which is approximately 2% points below the long-term summer climatology, whereas the picophytoplankton contribution increased correspondingly to ~36%. This transition was supported by shallower mixed layers (~30 m) and warmer surface waters (~28 °C), emphasizing how phytoplankton biomass could shift from larger to smaller size classes due to decreased upwelling and nutrient entrainment (Shunmugapandi et al. 2024).Taken together, the PSC climatologies (Figs. 3, 4 and 5) demonstrate that the Arabian Sea

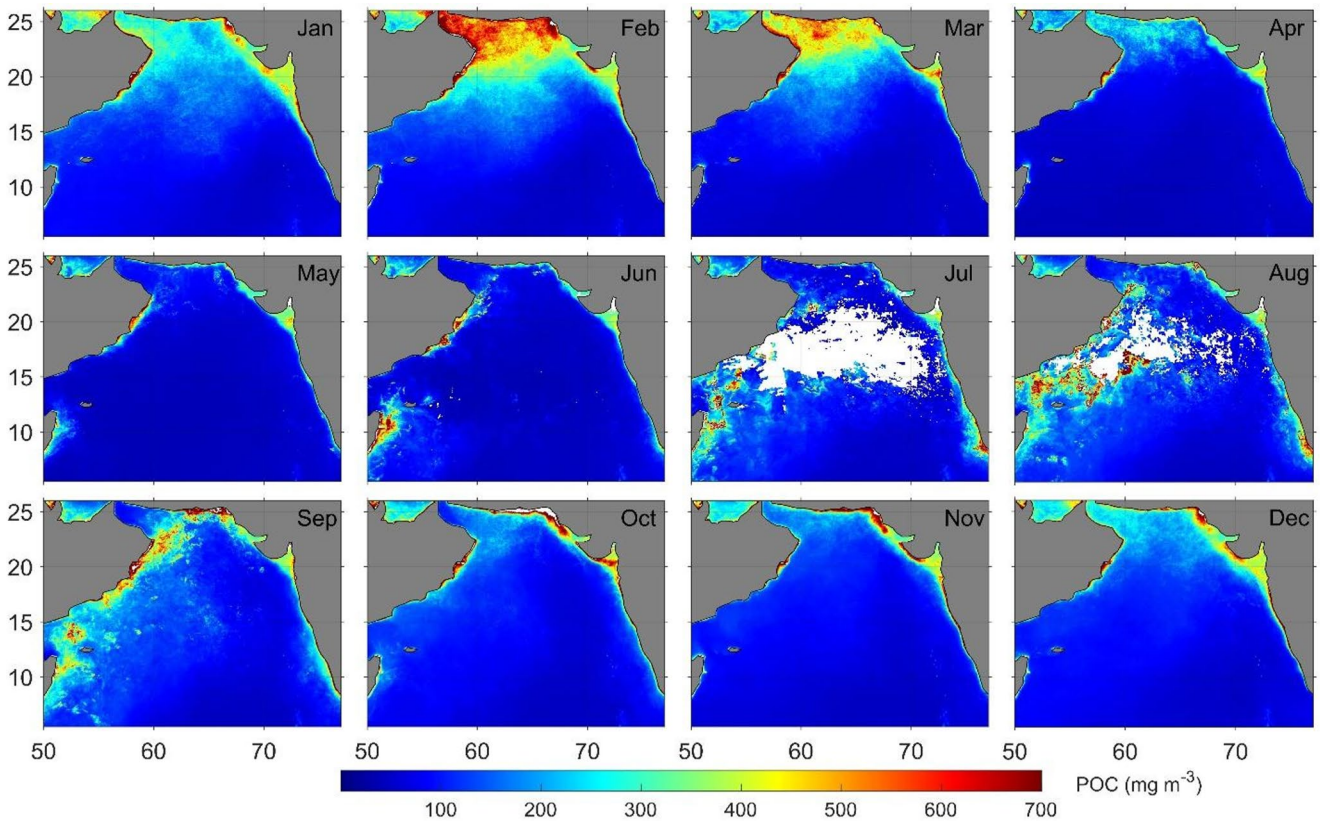


Fig. 8 Monthly climatology of surface particulate organic carbon (POC; mg m^{-3}) in the Arabian Sea, showing its spatial distribution and seasonal evolution throughout the annual cycle. The x-axis represents longitude (°E), and the y-axis represents latitude (°N)

undergoes pronounced seasonal restructuring between two contrasting community states: a microphytoplankton-dominated, diatom-driven, high-export regime during the two monsoons, and a picophytoplankton-dominated, microbial-loop-driven, low-export regime during the intermonsoon periods. The transitions between these states are mediated by nanophytoplankton-rich communities. This bimodal community shift, observed coherently across the entire basin, is the proximate cause of the strong seasonality of biological carbon export and trophic transfer to higher levels in the Arabian Sea food web.

Diatom dynamics and bloom evolution

The climatology of diatom spread area (Fig. 6) reveals two clearly demarcated diatom bloom periods, broadly congruent with but more sharply localized than the total microphytoplankton signal. The southwest monsoon diatom bloom (June-September) is centred on the upwelling zones along the Horn of Africa, the southern Arabian Peninsula, and the southwest Indian shelf, where the spatial extent of diatom-dominated spread area corresponds closely with elevated chl-*a* concentrations, generally exceeding 1.5 mg m^{-3} and locally surpassing 3 mg m^{-3} (Figs. 2 and 6). The bloom develops rapidly following the onset of upwelling-favourable winds in late May to early June, peaks in July-August coincident with the maximum cross-shore Ekman transport, and decays in September-October as wind stress relaxes and nutrient supply diminishes. The bloom edge progressively migrates offshore through summer, in association with the offshore propagation of upwelling filaments and the spread of nutrient-replete water by mesoscale eddies (Lévy et al. 2007). This sequence is the canonical eastern-boundary-like coastal upwelling diatom bloom, analogous in mechanism to the Benguela, Canary, and Peru-Chile systems.

The northeast-monsoon diatom bloom (December-February) is initiated in late November in the northern Arabian Sea and propagates southward and westward as convective mixing deepens through the winter. The spatial distribution of diatom spread area corresponds with elevated chl-*a* concentration, typically exceeding 1.0 mg m^{-3} across the northern interior in January, with peak values in coastal areas of the Indo-Pakistan shelf and the inner Gulf of Oman, where shelf-trapped enrichment processes amplify the offshore signal. The bloom decays in February-March, coincident with the cessation of convective mixing, the re-establishment of stratification, and, critically, the depletion of silicate from the surface layer following its drawdown by diatom growth

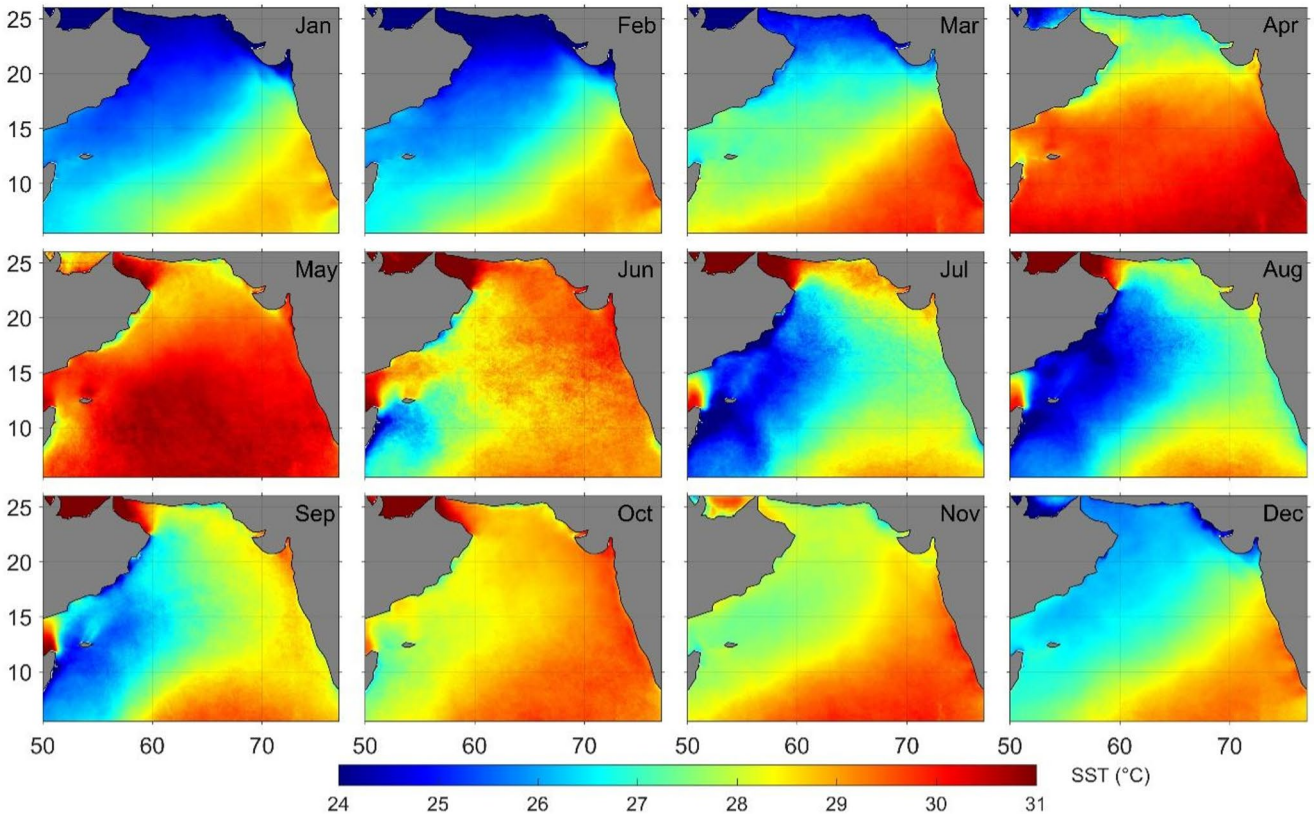


Fig. 9 Monthly climatology of sea surface temperature (SST; °C) in the Arabian Sea, showing its spatial distribution and seasonal evolution throughout the annual cycle. The x-axis represents longitude (°E), and the y-axis represents latitude (°N)

(Madhupratap et al. 1996; Wiggert et al. 2005; Lakshmi et al. 2021). The seasonal phasing of the diatom bloom thus differs fundamentally between the western boundary, where physical forcing (Ekman transport) is the primary driver, and the northern interior, where buoyancy loss and convective overturning dominate.

Diatom blooms in the Arabian Sea are silicate-limited in their termination phase, even though they may be initiated under nutrient-replete conditions. Si: N ratios in newly upwelled and convectively-mixed Arabian Sea water are typically near unity (Morrison et al. 1998), well below the 1.1–1.2 stoichiometry required by diatoms for balanced uptake (Brzezinski 1985). As blooms progress, silicate is depleted relative to nitrate, leading to a competitive disadvantage for diatoms compared with non-siliceous phytoplankton in the late bloom phase. These diatom bloom peaks persist until silicate is exhausted due to weakening mixing events and shallowing of the mixed layer (Xiang et al. 2019). This Si-N decoupling is a critical biogeochemical control that frames the subsequent succession to non-diatom communities. In the Arabian Sea, this succession increasingly favours GNS during the late winter monsoon, as discussed below.

Diatom export from the surface layer is also a major component of the Arabian Sea biological pump. Sediment trap observations from the U.S. and German JGOFS programmes documented strong, monsoonally synchronized pulses of biogenic silica and POC export to depth during both monsoons (Honjo et al. 1999; Haake et al. 1993), with diatoms providing the principal export vector. The persistence of substantial diatom blooms in the modern climatology (Fig. 6) confirms that diatoms remain a quantitatively important component of the Arabian Sea ecosystem despite the rise of GNS, although the relative balance has shifted (Gomes et al. 2014). Quantification of the long-term trends in this balance is an important objective for ongoing monitoring efforts.

Green *Noctiluca scintillans* dynamics and bloom evolution

The climatology of GNS surface spread (Fig. 7) reveals a strikingly distinct spatio-temporal pattern from that of diatoms. GNS is essentially absent from the Arabian Sea during the southwest monsoon and the spring intermonsoon, when surface waters are either too turbulent and freshly upwelled (southwest monsoon) or too nutrient-poor (spring

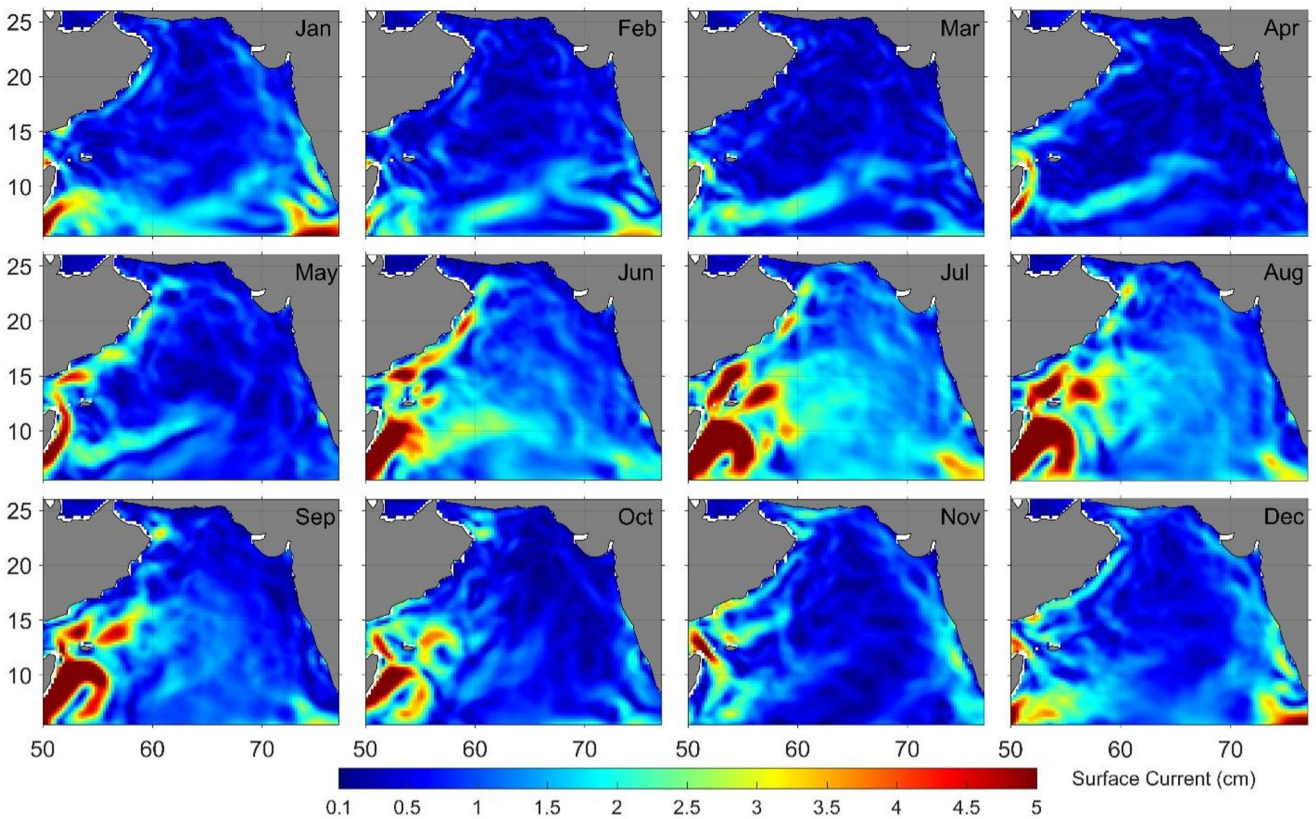


Fig. 10 Monthly climatology of sea surface current magnitude (cm s^{-1}) in the Arabian Sea, showing its spatial distribution and seasonal evolution throughout the annual cycle. The x-axis represents longitude (°E), and the y-axis represents latitude (°N)

intermonsoon) to support the bloom-forming mode of this species. Instead, GNS appears as a sparse, low-density signal in the eastern coastal Arabian Sea in November-December as the northeast monsoon begins, then expands rapidly through January, attaining its climatological peak in February-March across the central and northern Arabian Sea. By April, the bloom has largely collapsed, and GNS essentially disappears from the surface signal until the following winter.

This temporal sequence is systematically informative. The peak GNS bloom in February-March follows, by approximately one to two months, the peak diatom bloom of January (Fig. 6). It coincides with the cessation of convective mixing, the re-establishment of surface stratification (as evidenced by the SST climatology in Fig. 9), and the silicate depletion that terminates diatom growth. Under these conditions, the surface layer is nutrient-poor in silicate but still contains residual nitrogen, ammonium, and dissolved organic matter, much of it remineralized from sinking diatom debris and from the entrained waters. This combination is highly favourable for the mixotrophic GNS-endosymbiont system, which can simultaneously photosynthesize (via the symbiont) and ingest detritus and small phytoplankton (Hansen et al. 2004; Gomes et al. 2014). The hypoxic, ammonium-rich nature of the entrained water has been identified by Gomes et al. (2014) as the critical biogeochemical signature distinguishing the modern, GNS-favouring northeast monsoon regime from the historical, diatom-dominated regime that prevailed prior to the late 1990s.

Spatially, the climatological GNS bloom encompasses much of the central and northern Arabian Sea, with maximum occurence in the central region where convective mixing was deepest in the preceding months and where the OMZ shoals closest to the euphotic zone. The bloom shows a tendency to be advected southward and eastward by the prevailing northeast monsoon-driven currents (Fig. 10), occasionally reaching the southwest Indian coast and contributing to the well-known coastal "stench events" reported by Sahayak et al. (2005) and Padmakumar et al. (2012). The spatial coherence of the bloom across thousands of kilometres of open ocean, evident in Fig. 7, is one of the notable signatures of recent ecological change in the Arabian Sea.

The mixotrophy of GNS confers a competitive advantage that has only recently been fully appreciated in the Arabian Sea context. Unlike obligate autotrophs, which are constrained by inorganic nutrient availability, the GNS-symbiont system can sustain growth across a wide range of nutrient regimes by alternating between phototrophy

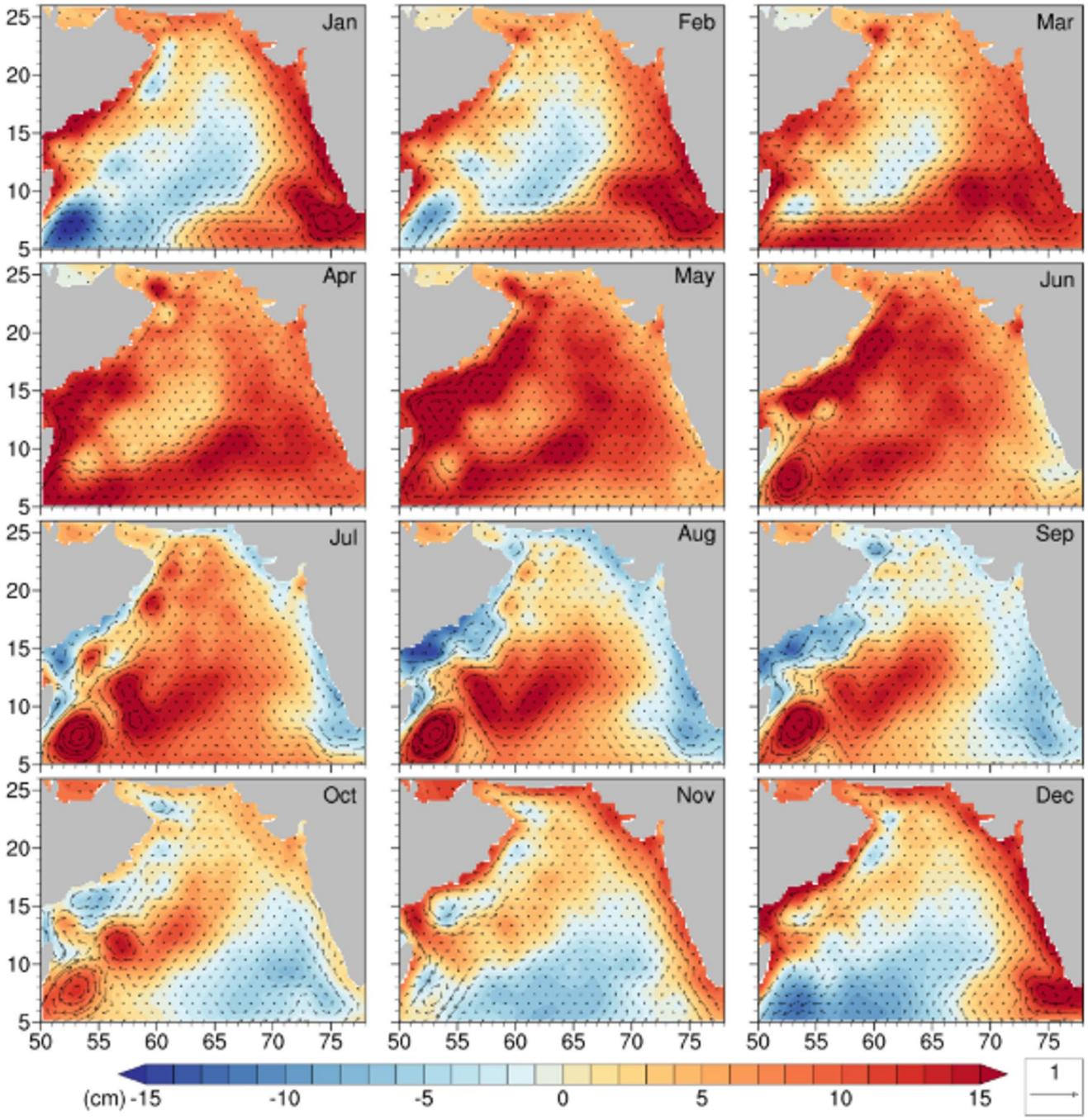


Fig. 11 Monthly climatology of sea level anomaly (cm) overlaid with geostrophic current fields in the Arabian Sea. The x-axis represents longitude (°E), and the y-axis represents latitude (°N)

and heterotrophy as conditions require. Its tolerance of low-oxygen, ammonium-rich water makes it pre-adapted to exploit precisely the kind of intermediate water that is increasingly outcropping in the modern Arabian Sea. Furthermore, GNS is largely refractory to traditional crustacean grazers, allowing its bloom biomass to accumulate to high levels with minimal top-down control (Kiørboe and Tiselius 1987; Padmakumar et al. 2012). The combination of bottom-up favourability and top-down release explains the explosive nature of the modern winter GNS blooms in the Arabian Sea.

Particulate organic carbon dynamics

The monthly climatology of POC (Fig. 8) closely mirrors that of total chl-*a* (Fig. 2) in spatio-temporal structure, with

POC values exceeding 200–300 mg m^{-3} along the southwest monsoon upwelling zones and across the convectively mixed northern interior in winter. This strong covariation confirms that surface POC in the Arabian Sea is dominated by suspended phytoplankton standing stock during bloom periods, consistent with global findings (Stramski et al. 2008; Kong et al. 2024). The chl-*a*-POC relationship, however, not strictly constant across the seasonal cycle: it tends to be higher during peak bloom conditions of southwest monsoon and winter productive periods, when fast-growing diatoms with high chlorophyll-per-cell content dominate, and decline during the intermonsoon and post-bloom periods, when slower-growing, nutrient-stressed cells, accumulated detritus, and heterotrophic biomass account for relatively more of the particulate carbon (Sathyendranath et al. 2009).

Two notable biogeochemical features emerge from the POC climatology. First, during the southwest monsoon, the offshore extension of high POC water along the Findlater Jet axis is more pronounced than the offshore extension of high chl-*a*, suggesting that biological carbon production along the western boundary is laterally exported into the central basin in the form of detritus and aged biogenic particles in addition to live phytoplankton. Second, the POC maximum during the northeast monsoon persists somewhat later in the season (often into March) than the corresponding chl-*a* maximum, an offset that is consistent with detrital carbon accumulation following diatom bloom collapse and with the contribution of the subsequent GNS bloom to surface POC. The GNS contribution is biogeochemically significant. Following bloom decline, the fate of GNS biomass remains poorly constrained. Available observations suggest limited direct export of intact cells, whereas carbon transfer through grazing by salps and jellyfish can enhance export via rapidly sinking faecal pellets; recycling within the upper water column may also be important (Gomes et al. 2014). The seasonal evolution of POC therefore encodes information not only on the magnitude of primary production but also on the partitioning of biological carbon between living and detrital pools and between exported and remineralized fractions.

Sea surface temperature and the physical context

The climatology of SST (Fig. 9) provides the essential physical framework for interpreting the biological patterns described above. Two prominent features stand out. The first is the pronounced cooling of the western Arabian Sea during the southwest monsoon, where SST falls to 24–25 °C along the Somali, Omani, and southwest Indian coasts in July-August. This cooling is the classical signature of monsoonal coastal upwelling, along-shore winds drive offshore Ekman transport, leading to upwelling of cold, nutrient-rich subsurface water into the surface layer (Lee et al. 2000). The strong SST front separating the cool upwelled water from warmer offshore water (often ~ 27–29 °C) marks the offshore edge of the bloom belt seen in the chl-*a* and POC climatologies, and the southward intrusion of cool water along the West Indian coast further coincides with the productive shelf bloom on the southwest Indian shelf.

The second prominent feature is the basin-wide cooling of surface waters in the northern Arabian Sea during the northeast monsoon. SST declines from a peak of ~ 29–30 °C in October to ~ 24–25 °C in February north of 18°N. This cooling is driven primarily by net surface heat loss to the cold, dry continental atmosphere, supplemented by latent and sensible heat fluxes associated with the northeast monsoon winds. The thermohaline buoyancy loss reduces upper-ocean stratification and triggers convective mixing, deepening the mixed layer to 100–125 m in the northern interior and entraining nutrients from the underlying nutricline. The peak of the northern Arabian Sea bloom lags the period of most intense northeast-monsoon surface cooling and convective overturning by approximately one month. Net surface heat loss and mixed-layer deepening are strongest as SST falls most rapidly, around December to January, whereas the associated chl-*a* maximum is attained in January-February. This trailing of the biological response behind the physical forcing, rather than a coincidence of the two, provides a clear physical-biological coupling diagnostic. Following the cessation of cooling in March, surface waters begin to rewarm and restratify, thereby terminating convective mixing and reducing nutrient supply, thus concluding the diatom bloom and ushering in the late-winter GNS succession.

The intermonsoon SST distributions show a smooth, basin-wide warming, with values exceeding 30 °C across the central and southern Arabian Sea in May before the southwest monsoon onset and a more modest secondary warming in October-November before the northeast monsoon onset. These warm intermonsoon SSTs underlie the strong stratification and nutrient limitation that produce the spring and fall oligotrophic chl-*a* minima. The progressive warming trend documented for the Arabian Sea over recent decades, attributed to rapid Indian Ocean warming under anthropogenic climate change (Roxy et al. 2016), has contributed to a strengthening of stratification during the warm seasons and suppress vertical nutrient exchange, and create thermally stable surface layers that favour the proliferation of heat-tolerant, opportunistic planktonic species (Moore et al. 2008; Gobler et al. 2017).

Sea surface circulation and bloom advection

The climatology of sea surface currents (Fig. 10) confirms the seasonal reversal of surface circulation that defines the Arabian Sea. During the southwest monsoon, the Findlater Jet drives strong northward surface current along the western Arabian Sea, forming the Somali Current, while the wind-driven currents along the Omani shelf. These currents are associated with the basin-scale summer monsoon circulation and southward flowing East Arabian Current along the West coast of India. This circulation pattern produces strong cross-shore Ekman transport along the western boundary and offshore advection of upwelled, productive water in the form of cold-water filaments and mesoscale eddies, mechanisms that are visible in the chl-*a*, POC, and diatom climatologies as offshore extensions of the bloom belt.

During the northeast monsoon, the surface circulation reverses. The Somali Current weakens and reverses, flowing southward; the West Indian Coastal Current flows northward along the Indian shelf and around the head of the basin; and the basin-wide circulation becomes anticlockwise. Surface speeds in the open central and northern Arabian Sea are generally moderate, consistent with the wind-driven Ekman flow associated with northeast monsoon winds. Satellite observations indicate that the winter diatom bloom develops across the northern Arabian Sea, with earlier observations suggesting an eastward progression from the western northern Arabian Sea, followed by the development and spatial expansion of GNS blooms (Lotliker et al. 2020). The resulting GNS bloom can extend across the northern Arabian Sea between the west coast of India and Oman, although the relative contributions of local growth and horizontal advection to this spatial progression remain unresolved.

The intermonsoon periods show much weaker surface flows and a diffuse, transitional circulation pattern. The combination of weak winds, weak currents, and warm, stratified surface waters produces a quiescent physical regime that supports the oligotrophic, picophytoplankton-dominated communities documented above. The transition from intermonsoon to monsoon circulation represents a dramatic and rapid reorganization of the Arabian Sea surface waters.

The diatom-Green Noctiluca shift: mechanisms and implications

The juxtaposition of the diatom (Fig. 6) and GNS (Fig. 7) climatologies, set against the physical (Figs. 9 and 10) and biogeochemical (Figs. 2 and 8) context, provides a coherent picture of the modern winter monsoon ecological regime in the Arabian Sea: an early-winter diatom bloom is followed, with a lag of approximately one month, by a late-winter GNS that occupies essentially the same spatial domain. This temporal succession represents a fundamental restructuring of the winter Arabian Sea ecosystem relative to its historical diatom-dominated state and is the most striking ecological signal in the basin in recent decades (Goes et al. 2018; Gomes et al. 2014).

Several non-exclusive mechanisms have been proposed to explain the rise of GNS in the modern Arabian Sea. Gomes et al. (2014) advanced the hypoxia hypothesis, arguing that the shoaling and lateral expansion of the OMZ delivers low-oxygen, organic-matter-laden water to the surface during convective mixing, conditions under which the mixotrophic GNS-symbiotic system has a competitive advantage over obligately autotrophic diatoms. However, oceanic GNS blooms have also been observed in the absence of hypoxia (Lotliker et al. 2018), and shallow convective mixing has been proposed as an alternative trigger (Sarma et al. 2019). Roxy et al. (2016) emphasized the role of progressive surface warming, which strengthens stratification, weakens convective mixing, reduces silicate supply to the surface (which may be due to silicate has a deeper remineralization horizon than nitrate), and thus tilts the silicate-to-nitrate balance against diatoms. Goes et al. (2005) earlier suggested that warming of the Eurasian land mass intensifies the southwest monsoon and thus enhances productivity, but recent re-evaluations (Gomes et al. 2014) have argued for a more complex, possibly opposite, response in winter.

The picture that emerges from the present climatological synthesis is one of an Arabian Sea ecosystem in transition. The fundamental seasonal architecture of monsoon-driven productivity is preserved, but its biological expression has been substantially modified over the past decades, with the rise of GNS as a major winter bloom-former. The key satellite-derived parameters analysed here, total chl-*a*, the three PSCs, diatom spread area, GNS spread area, POC, SST, and surface currents, and SLA together provide a comprehensive observational framework for tracking this transition into the future and for evaluating the ecosystem response to continued climate change.

Regional variability between the eastern and central Arabian Sea

As the present analysis spans the entire basin, it is important to distinguish the contrasting environmental controls that operate in the eastern and central Arabian Sea. The eastern Arabian Sea, adjoining the southwest Indian shelf, is a comparatively shallow, coastally influenced regime in which productivity is modulated by seasonal coastal upwelling during the southwest-monsoon, by shelf and riverine nutrient inputs, and by mud-bank and buoyancy-driven processes near the coast (Jyothibabu et al. 2008; Karnan et al. 2017; Albin et al. 2022).

During the southwest-monsoon, coastal upwelling along the southeast Arabian Sea boundary develops in the south and then progresses northward. Before upwelling, the stratified, nitrate-depleted upper ocean, maintained by surface heating and the intrusion of low-salinity Bay of Bengal water, is dominated by picophytoplankton. At peak upwelling, nutrient entrainment drives a marked shift towards large-sized micro- and mesophytoplankton. As the strength of the upwelling decreases, the community reverts to nano-, and picophytoplankton assemblage during post-upwelling phase (Albin et al. 2024). The eastern margin thus differs from broadly distributed open-ocean response of the central basin, being governed instead by a strong coast-to-offshore gradient and pronounced seasonal succession. Seasonal productivity contrasts are also evident, the stratified southeastern Arabian Sea remains comparatively less productive during the northeast-monsoon, whereas southwest-monsoon upwelling raises chl-*a* and primary production several-fold (Albin et al. 2022).

During the northeast-monsoon, winter convective mixing in the northeastern Arabian Sea initially boosts nanophytoplankton and marginally enriches surface waters (Albin et al. 2022). Here, winter convective mixing is comparatively shallow, stratification re-establishes early, and both the diatom and GNS blooms tend to occur as narrower, near-shore features that are frequently advected along the coast by the northward West Indian Coastal Current. Shallow mixing may supply phosphate and nitrate without reaching the silicicline, resulting in low Si: N conditions that promote microphytoplankton-sized blooms of the GNS and suppress diatoms (Sarma et al. 2019).

The central Arabian Sea, by contrast, is a deep, open-ocean regime whose winter productivity is driven by basin-scale convective overturning forced by continental-air buoyancy loss; there, the mixed layer deepens to 100–125 m, nutrient entrainment is basin-wide rather than shelf-constrained, and the resulting diatom bloom and subsequent GNS bloom attain their greatest spatial coherence and highest open-ocean abundance (Madhupratap et al. 1996; Kumar et al. 2000, 2001). Region-specific variations are additionally observed in the emergence and spread of GNS blooms. Observations from 2018 to 2021 along the southeastern Arabian Sea coast suggest that recurrent winter blooms may be seeded by cells of GNS and are transported from the southwestern Bay of Bengal around Sri Lanka and into the west coast of India by the seasonally reversing East India Coastal Currents (Sathish et al. 2023). As a result, compared with the large blooms observed over the northern open Arabian Sea, these blooms are narrower, more transient, and strongly influenced by coastal advection. The development and restructuring of diatom and GNS blooms in the northern and north-central interior have been collectively controlled by winter mixing, intermittent restratification, mesoscale circulation, nutrient stoichiometry, and prey availability (Gomes et al. 2014; Lotliker et al. 2018; Thoppil 2023).

The regional contrasts outlined above ultimately arise from the seasonally reversing surface circulation, which sets the depth of mixing, the nutrient-supply pathways, and the advective redistribution of blooms across the eastern and central basin. The SLA-overlaid geostrophic-current fields resolve this circulation (Fig. 11), which provides important physical controls on the distribution of diatom/GNS blooms (Figs. 6 and 7). During winter (December-February), reduced shortwave radiation and enhanced evaporation driven by dry northeasterly continental winds cool and increase the salinity of the northern Arabian Sea, producing cooler, saline surface waters north of 15°N. The resulting increase in surface-water density promotes convective mixing and deepening of the upper ocean (Kumar and Prasad 1996; Kumar et al. 2001). These circulation features favour upwelling, vertical displacement of subsurface waters, and enhanced nutrient availability, while strong wintertime convective mixing further deepens the mixed layer and entrains nutrients into the euphotic zone (Kumar and Narvekar 2005). The combination of vertical nutrient supply and horizontal advection therefore provides favourable conditions for the extensive distribution of winter diatoms and GNS. During the spring (March-May), maximum insolation and peak SST allow the progressive development of a surface-stratified, shallow mixed layer, accompanied by a reduction in the spatial extent of diatom-rich regions (Kumar and Narvekar 2005). Anticyclonic circulation associated with positive SLA promotes downwelling and retention of surface waters, thereby limiting vertical nutrient replenishment. The associated horizontal currents can nevertheless redistribute phytoplankton and nutrient-rich waters, producing localized patches of enhanced diatom occurrence. During the summer monsoon (June-September), the circulation becomes strongly influenced by monsoon-driven winds and currents, leading to the observed cooler SST. Further-enhanced low-level Findlater Jet activity intensified wind-driven Ekman divergence, thereby promoting open-ocean upwelling with a shallow mixed layer (Bauer et al. 1991; Kumar et al. 2001). These processes contribute to the spatially heterogeneous distribution of diatoms and GNS, particularly over the western and northern Arabian Sea, through enhanced horizontal advection, coastal and open-ocean upwelling, and eddy-mediated transport. During October-November, weakening summer stratification and the transition toward the winter circulation regime favour renewed vertical exchange and nutrient replenishment. The increasing diatom/GNS occurrence over the northern and central Arabian Sea is therefore

likely associated with the combined effects of convective mixing, mesoscale circulation, and horizontal advection.

Conclusion

The present study has used a multi-parameter MODIS-Aqua climatology to characterize the spatio-temporal dynamics of total chl-*a*, three PSCs, diatoms, GNS, POC, SST, sea surface currents and SLA in the Arabian Sea. The integrated analysis confirms and extends earlier findings, while providing a coherent observational framework for understanding the contemporary ecosystem and its ongoing reorganization. The salient outcomes of this study are as follows.

First, the Arabian Sea exhibits a strongly bimodal annual cycle of phytoplankton biomass, with peak chl-*a* and POC concentrations during both the southwest (June-September) and northeast (December-February) monsoons, separated by oligotrophic intermonsoons. The southwest monsoon bloom is concentrated along the upwelling-fringed Somali, Oman, and southwest Indian coasts, while the northeast-monsoon bloom is a basin-wide, convectively-driven feature of the northern interior. POC closely tracks chl-*a* in space and time but exhibits lagged decay and an offshore extension that reflects the contributions of detrital and heterotrophic carbon pools. Second, the size-class structure of the phytoplankton community oscillates between a microphytoplankton-dominated, diatom-driven, high-export state during monsoon blooms and a picophytoplankton-dominated, microbial-loop-driven, low-export state during intermonsoons. Nanophytoplankton mediate transitions and are particularly important in mesotrophic conditions during the early and late phases of the bloom. Third, diatoms remain the major bloom-forming microphytoplankton in both monsoons, with their spatial extent and bloom phenology controlled jointly by physical nutrient supply (upwelling and convective mixing) and silicate availability. Diatom blooms terminate primarily through silicate depletion, setting the stage for non-diatom successors. Fourth, GNS attains its peak surface occurrence during late winter (February-March) in the central and northern Arabian Sea, immediately following the diatom bloom, in a temporal succession that is best explained by the joint effects of silicate depletion, post-bloom stratification, and the mixotrophic capabilities of the GNS-symbiont symbiosis. Fifth, the physical climatology of SST and surface currents provides the essential context for interpreting biological patterns. Monsoonal cooling (by upwelling in summer and convective loss in winter) and the seasonal reversal of surface circulation jointly govern the timing, location, and offshore propagation of phytoplankton blooms. The two climatologies together demonstrate the close coupling between physical forcing and biological response that characterizes monsoonal ecosystems. Sixth, the documented diatom-to-GNS shift carries significant implications for the Arabian Sea biological carbon pump, food web, and pelagic fisheries. Continued progression of the shift, driven by ongoing surface warming, intensifying stratification, and the further expansion of intermediate-water hypoxia, may influence biological carbon export, redirect energy flow through gelatinous and microbial pathways, and the prey base available to commercially important fish stocks. These prospects underscore the importance of sustained, multi-parameter ocean-colour and physical observations of the Arabian Sea and motivate further research on the long-term trends, the underlying biogeochemical mechanisms, and the regional and global implications of this ongoing ecological transition.

The present study is subject to uncertainties associated with the absence of direct nutrient, oxygen, and grazing observations limits assessment of the underlying ecological mechanisms. Furthermore, the climatological, satellite-based analysis does not resolve vertical processes or establish temporal trends and systematic relationships between diatom and GNS dynamics. Therefore, the study recommends seasonal in situ observations throughout the water column to validate satellite-derived phytoplankton distributions and better resolve the roles of nutrients, oxygen, grazing, and vertical physical processes in regulating diatom and GNS dynamics. Continued integration of MODIS-Aqua observations with successor missions (notably PACE, OCI, and Sentinel-3 OLCI), high-frequency in situ time series, biogeochemical modelling, and biological process studies will be essential for monitoring the trajectory of the Arabian Sea ecosystem under the combined pressures of climate change and direct human impacts.

Supplementary Information The online version contains supplementary material available at https://doi.org/10.1007/s00227-026-04987-3.

Acknowledgements The authors express their sincere gratitude to the authorities of their respective organizations for their support and encouragement in conducting this study. The authors gratefully acknowledge the NASA Ocean Biology Distributed Active Archive Center (OB.DAAC) for providing open access to MODIS-Aqua Level-3 ocean colour and sea surface temperature (SST) products, and the Earth and Space Research (ESR) team for making the OSCAR surface current data available. Appreciation is also extended to the developers of the OC3M, POC, PSC, and diatom-retrieval algorithms used in this work. The present study forms part of the doctoral research undertaken by the second author, Ayana, and the third author, Susmita. This publication is an INCOIS contribution no. 736. The first author gratefully acknowledges the India-Japan Circulation of Talented Youths in Science Programme (LOTUS) Fellowship under the Japan Science and Technology Agency (JST), Japan.

Author contributions **AKJ**: Conceptualization, Data curation, Formal analysis, Methodology, Software, Investigation, Visualization, Writing – original draft; **SA**: Investigation, Formal analysis, Writing - original

draft; **SR**: Investigation, Formal analysis, Writing - original draft; **SS**: Formal analysis, Investigation, Writing - original draft; **SKB**: Conceptualization, Supervision, Formal analysis, Investigation, Writing - original draft; **AS**: Supervision, Methodology, Software, Writing – review & editing, **TMB**: Supervision, Writing – review & editing. All authors read and approved the final manuscript.

Funding No funding has been received for this work.

Data availability The datasets used in this study were obtained from NASA's Physical Oceanography Distributed Active Archive Center (PO.DAAC) and Ocean Color Web portals, including the OSCAR surface current dataset and MODIS-Aqua ocean colour products.

Declarations

Ethics approval and consent to participate Not applicable.

Consent for publication Not applicable.

Competing interests The authors declare that they have no known competing financial or non-financial interests or personal relationships that could have appeared to influence the work reported in this paper.

References

Albin KJ, Jyothibabu R, Alok KT, Santhikrishnan S, Sarath S, Sudheesh V, Sherin CK, Balachandran KK, Asha Devi CR, Gupta GVM (2022) Distinctive phytoplankton size responses to the nutrient enrichment of coastal upwelling and winter convection in the eastern Arabian Sea. Prog Oceanogr 203:102779. https://doi.org/10.1016/j.pocean.2022.102779

Albin KJ, Jyothibabu R, Alok KT, Santhi Krishnan S, Sherin CK, Gupta GVM (2024) Effects of seasons and successive upwelling phases on phytoplankton size classes in the Southeast Arabian Sea. Mar Environ Res 198:106568. https://doi.org/10.1016/j.marenvres.2024.106568

Balch WM, Haxo FT (1984) Spectral properties of *Noctiluca miliaris* Suriray, a heterotrophic dinoflagellate. J Plankton Res 6:515–525. https://doi.org/10.1093/plankt/6.3.515

Baliarsingh SK, Lotliker AA, Sudheesh V, Samanta A, Das S, Vijayan AK (2018) Response of phytoplankton community and size classes to green *Noctiluca* bloom in the northern Arabian Sea. Mar Pollut Bull 129:222–230. https://doi.org/10.1016/j.marpolbul.2018.02.031

Banse K (1987) Seasonality of phytoplankton chlorophyll in the central and northern Arabian Sea. Deep Sea Res Part Oceanogr Res Pap 34:713–723. https://doi.org/10.1016/0198-0149(87)90032-X

Banse K, Naqvi SWA, Narvekar PV, Postel JR, Jayakumar DA (2014) Oxygen minimum zone of the open Arabian Sea: variability of oxygen and nitrite from daily to decadal timescales. Biogeosciences 11:2237–2261. https://doi.org/10.5194/bg-11-2237-2014

Bauer S, Hitchcock GL, Olson DB (1991) Influence of monsoonally-forced Ekman dynamics upon surface layer depth and plankton biomass distribution in the Arabian Sea. Deep Sea Res Part Oceanogr Res Pap 38:531–553. https://doi.org/10.1016/0198-0149(91)90062-K

Bharathi MD, Muthukumar C, Sathishkumar RS, Ramu K, Ramana Murthy MV (2023) First report on the occurrence of *Gonyaulax polygramma* bloom during the onset of *Noctiluca scintillans* bloom along the Tuticorin coast, southeast coast of India. Mar Pollut Bull 195:115523. https://doi.org/10.1016/j.marpolbul.2023.115523

Bonjean F, Lagerloef GSE (2002) Diagnostic model and analysis of the surface currents in the tropical Pacific Ocean. J Phys Oceanogr 32:2938–2954. https://doi.org/10.1175/1520-0485(2002)032%3C2938:DMAAOT%3E2.0.CO;2

Brewin RJW, Sathyendranath S, Hirata T, Lavender SJ, Barciela RM, Hardman-Mountford NJ (2010) A three-component model of phytoplankton size class for the Atlantic Ocean. Ecol Model 221:1472–1483. https://doi.org/10.1016/j.ecolmodel.2010.02.014

Brewin RJW, Hardman-Mountford NJ, Lavender SJ, Raitsos DE, Hirata T, Uitz J, Devred E, Bricaud A, Ciotti A, Gentili B (2011) An intercomparison of bio-optical techniques for detecting dominant phytoplankton size class from satellite remote sensing. Remote Sens Environ 115:325–339. https://doi.org/10.1016/j.rse.2010.09.004

Brewin RJW, Sathyendranath S, Jackson T, Barlow R, Brotas V, Airs R, Lamont T (2015) Influence of light in the mixed-layer on the parameters of a three-component model of phytoplankton size class. Remote Sens Environ 168:437–450. https://doi.org/10.1016/j.rse.2015.07.004

Brzezinski MA (1985) The Si:C:N ratio of marine diatoms: interspecific variability and the effect of some environmental variables. J Phycol 21:347–357. https://doi.org/10.1111/j.0022-3646.1985.00347.x

Chowdhury M, Biswas H, Silori S, Sharma D (2024) Spatiotemporal variability in phytoplankton size class modulated by summer monsoon wind forcing in the central Arabian Sea. J Geophys Res Oceans 129. https://doi.org/10.1029/2023JC019880.e2023JC019880

Ciotti AM, Bricaud A (2006) Retrievals of a size parameter for phytoplankton and spectral light absorption by colored detrital matter from water-leaving radiances at SeaWiFS channels in a continental shelf region off Brazil. Limnol Oceanogr Methods 4:237–253. https://doi.org/10.4319/lom.2006.4.237

Cushing DH (1989) A difference in structure between ecosystems in strongly stratified waters and in those that are only weakly stratified. J Plankton Res 11:1–13. https://doi.org/10.1093/plankt/11.1.1

Devred E, Sathyendranath S, Stuart V, Maass H, Ulloa O, Platt T (2006) A two-component model of phytoplankton absorption in the open ocean: theory and applications. J Geophys Res Oceans 111:C03011. https://doi.org/10.1029/2005JC002880

Dwivedi R, Rafeeq M, Smitha BR, Padmakumar KB, Thomas LC, Sanjeevan VN, Prakash P, Raman M (2015) Species identification of mixed algal bloom in the Northern Arabian Sea using remote sensing techniques. Environ Monit Assess 187:51. https://doi.org/10.1007/s10661-015-4291-2

Egge JK, Aksnes DL (1992) Silicate as regulating nutrient in phytoplankton competition. Mar Ecol Prog Ser 83:281–289. https://doi.org/10.3354/meps083281

Falkowski PG, Woodhead AD, Vivirito K (eds) (1992) Primary productivity and biogeochemical cycles in the sea, vol 43. Springer, New York. https://doi.org/10.1007/978-1-4899-0762-2

Furuya K, Saito H, Sriwoon R, Omura T, Furio EE, Borja VM, Lirdwitayaprasit T (2006) Vegetative growth of *Noctiluca scintillans* containing the endosymbiont *Pedinomonas noctilucae*. Afr J Mar Sci 28:305–308. https://doi.org/10.2989/18142320609504167

Garrison DL, Gowing MM, Hughes MP, Campbell L, Caron DA, Dennett MR, Shalapyonok A, Olson RJ, Landry MR, Brown SL, Liu HB, Azam F, Steward GF, Ducklow HW, Smith DC (2000) Microbial food web structure in the Arabian Sea: a US JGOFS study. Deep Sea Res Part II Top Stud Oceanogr 47:1387–1422. https://doi.org/10.1016/S0967-0645(99)00148-4

Gobler CJ, Doherty OM, Hattenrath-Lehmann TK, Griffith AW, Kang Y, Litaker RW (2017) Ocean warming since 1982 has expanded

the niche of toxic algal blooms in the North Atlantic and North Pacific oceans. Proc Natl Acad Sci USA 114:4975–4980. https://doi.org/10.1073/pnas.1619575114

Goes JI, Thoppil PG, Gomes HR, Fasullo JT (2005) Warming of the Eurasian landmass is making the Arabian Sea more productive. Science 308:545–547. https://doi.org/10.1126/science.1106610

Goes JI, Gomes HR, Al-Hashimi K, Buranapratheprat A (2018) Ecological drivers of green *Noctiluca* blooms in two monsoonal-driven ecosystems. In: Glibert PM, Berdalet E, Burford MA, Pitcher GC, Zhou M (eds) Global ecology and oceanography of harmful algal blooms. Ecological Studies, vol 232. Springer, Cham, pp 327–336. https://doi.org/10.1007/978-3-319-70069-4_17

Goldenberg SU, Taucher J, Fernandez-Mendez M, Ludwig A, Arístegui J, Baumann M, Ortiz J, Stuhr A, Riebesell U (2022) Nutrient composition (Si:N) as driver of plankton communities during artificial upwelling. Front Mar Sci 9:1015188. https://doi.org/10.3389/fmars.2022.1015188

Gomes HR, Goes JI, Matondkar SGP, Buskey EJ, Basu S, Parab S, Thoppil P (2014) Massive outbreaks of *Noctiluca scintillans* blooms in the Arabian Sea due to spread of hypoxia. Nat Commun 5:4862. https://doi.org/10.1038/ncomms5862

Haake B, Ittekkot V, Rixen T, Ramaswamy V, Nair RR, Curry WB (1993) Seasonality and interannual variability of particle fluxes to the deep Arabian Sea. Deep Sea Res Part I Oceanogr Res Pap 40:1323–1344. https://doi.org/10.1016/0967-0637(93)90114-I

Hansen PJ, Miranda L, Azanza R (2004) Green *Noctiluca scintillans*: a dinoflagellate with its own greenhouse. Mar Ecol Prog Ser 275:79–87. https://doi.org/10.3354/meps275079

Hirata T, Aiken J, Hardman-Mountford N, Smyth TJ, Barlow RG (2008) An absorption model to determine phytoplankton size classes from satellite ocean colour. Remote Sens Environ 112:3153–3159. https://doi.org/10.1016/j.rse.2008.03.011

Hirata T, Hardman-Mountford NJ, Brewin RJW, Aiken J, Barlow R, Suzuki K, Isada T, Howell E, Hashioka T, Noguchi-Aita M, Yamanaka Y (2011) Synoptic relationships between surface chlorophyll-a and diagnostic pigments specific to phytoplankton functional types. Biogeosciences 8:311–327. https://doi.org/10.5194/bg-8-311-2011

Honjo S, Dymond J, Prell W, Ittekkot V (1999) Monsoon-controlled export fluxes to the interior of the Arabian Sea. Deep Sea Res Part II Top Stud Oceanogr 46:1859–1902. https://doi.org/10.1016/S0967-0645(99)00047-8

Jyothibabu R, Devi CA, Madhu NV, Sabu P, Jayalakshmy KV, Jacob J, Habeebrehman H, Prabhakaran MP, Balasubramanian T, Nair KKC (2008) The response of microzooplankton (20–200 µm) to coastal upwelling and summer stratification in the southeastern Arabian Sea. Cont Shelf Res 28:653–671. https://doi.org/10.1016/j.csr.2007.12.001

Karnan C, Jyothibabu R, Arunpandi N, Jagadeesan L, Muraleedharan KR, Pratihari AK, Balachandran KK, Naqvi SWA (2017) Discriminating the biophysical impacts of coastal upwelling and mud banks along the southwest coast of India. J Mar Syst 172:24–42. https://doi.org/10.1016/j.jmarsys.2017.02.012

Khan H, Govil P, Panchang R, Agrawal S, Kumar P, Kumar B, Verma D (2023) Surface and thermocline ocean circulation intensity changes in the western Arabian Sea during ~ 172 kyr. Quat Sci Rev 311:108133. https://doi.org/10.1016/j.quascirev.2023.108133

Kiørboe T, Tiselius PT (1987) Gut clearance and pigment destruction in a herbivorous copepod, *Acartia tonsa*, and the determination of in situ grazing rates. J Plankton Res 9:525–534. https://doi.org/10.1093/plankt/9.3.525

Koné V, Aumont O, Lévy M, Resplandy L (2009) Physical and biogeochemical controls of the phytoplankton seasonal cycle in the Indian Ocean: a modeling study. In: Wiggert JD, Hood RR, Naqvi SWA, Brink KH, Smith SL (eds) Indian Ocean biogeochemical processes and ecological variability. Geophys Monogr Ser 185:147–166. American Geophysical Union. https://doi.org/10.1029/2008GM000700

Kong CE, Sathyendranath S, Jackson T, Stramski D, Brewin RJW, Kulk G, Jönsson BF, Loisel H, Galí M, Le C (2024) Comparison of ocean-colour algorithms for particulate organic carbon in global ocean. Front Mar Sci 11:1309050. https://doi.org/10.3389/fmars.2024.1309050

Kumar SP, Narvekar J (2005) Seasonal variability of the mixed layer in the central Arabian Sea and its implication on nutrients and primary productivity. Deep Sea Res Part II Top Stud Oceanogr 52:1848–1861. https://doi.org/10.1016/j.dsr2.2005.06.002

Kumar SP, Prasad TG (1996) Winter cooling in the northern Arabian Sea. Curr Sci 71:834–841

Kumar SP, Madhupratap M, Kumar MD, Gauns M, Muraleedharan PM, Sarma VVSS, De Souza SN (2000) Physical control of primary productivity on a seasonal scale in central and eastern Arabian Sea. J Earth Syst Sci 109:433–441. https://doi.org/10.1007/BF02708331

Kumar SP, Madhupratap M, Kumar MD, Muraleedharan PM, De Souza SN, Gauns M, Sarma VVSS (2001) High biological productivity in the central Arabian Sea during the summer monsoon driven by Ekman pumping and lateral advection. Curr Sci 81:1633–1638

Kumar SP, Roshin RP, Narvekar J, Kumar PD, Vivekanandan E (2010) What drives the increased phytoplankton biomass in the Arabian Sea? Curr Sci 99:101–106

Lachkar Z, Lévy M, Smith KS (2019) Strong intensification of the Arabian Sea oxygen minimum zone in response to Arabian Gulf warming. Geophys Res Lett 46:5420–5429. https://doi.org/10.1029/2018GL081631

Lakshmi RS, Prakash S, Lotliker AA, Baliarsingh SK, Samanta A, Mathew T, Chatterjee A, Sahu BK, Nair TB (2021) Physicochemical controls on the initiation of phytoplankton bloom during the winter monsoon in the Arabian Sea. Sci Rep 11:13448. https://doi.org/10.1038/s41598-021-92897-3

Latasa M, Bidigare RR (1998) A comparison of phytoplankton populations of the Arabian Sea during the Spring Intermonsoon and Southwest Monsoon of 1995 as described by HPLC-analyzed pigments. Deep Sea Res Part II Top Stud Oceanogr 45:2133–2170. https://doi.org/10.1016/S0967-0645(98)00066-6

Lee CM, Jones BH, Brink KH, Fischer AS (2000) The upper-ocean response to monsoonal forcing in the Arabian Sea: seasonal and spatial variability. Deep Sea Res Part II Top Stud Oceanogr 47:1177–1226. https://doi.org/10.1016/S0967-0645(99)00141-1

Lévy M, Shankar D, André JM, Shenoi SSC, Durand F, de Boyer Montégut C (2007) Basin-wide seasonal evolution of the Indian Ocean's phytoplankton blooms. J Geophys Res Oceans 112:C12014. https://doi.org/10.1029/2007JC004090

Liu Y, Zhang Y, Yao H, Zheng Z, Zhao W, Lin G (2025) Analysis on bacterial community of *Noctiluca scintillans* algal blooms near Pingtan Island, China. Biology 14:101. https://doi.org/10.3390/biology14010101

Lotliker AA, Baliarsingh SK, Trainer VL, Wells ML, Wilson C, Udaya Bhaskar TVS, Samanta A, Shahimol SR (2018) Characterization of oceanic *Noctiluca* blooms not associated with hypoxia in the Northeastern Arabian Sea. Harmful Algae 74:46–57. https://doi.org/10.1016/j.hal.2018.03.008

Lotliker AA, Baliarsingh SK, Samanta A, Varaprasad V (2020) Growth and decay of high-biomass algal bloom in the northern Arabian Sea. J Indian Soc Remote Sens 48:465–471. https://doi.org/10.1007/s12524-019-01094-3

Madhupratap M, Prasanna Kumar S, Bhattathiri PMA, Dileep Kumar M, Raghukumar S, Nair KKC, Ramaiah N (1996) Mechanism of the biological response to winter cooling in the northeastern Arabian Sea. Nature 384:549–552. https://doi.org/10.1038/384549a0

Manigandan V, Muthukumar C, Shah C, Logesh N, Sivadas SK, Ramu K, Murthy MR (2024) Phylogenetic affiliation of *Pedinomonas*

noctilucae and green *Noctiluca scintillans* nutritional dynamics in the Gulf of Mannar, Southeastern Arabian Sea. Protist 175:126019. https://doi.org/10.1016/j.protis.2024.126019

Mariasingarayan Y, Gunasekaran K, Renganathan M, Ayyappan S (2025) Devastating impact of *Noctiluca scintillans* ((Macartney) Kofoid & Swezy, 1921) bloom on marine fishes in the Gulf of Mannar, India. Discover Oceans 2:36. https://doi.org/10.1007/s44289-025-00074-5

Matondkar SGP, Basu S, Parab SG, Pednekar S, Dwivedi RM, Raman M, Goes JI, Gomes H (2012) The bloom of the dinoflagellate (*Noctiluca miliaris*) in the North Eastern Arabian Sea: Ship and Satellite study. In Proceedings of the 11th Biennial Conference of Pan Ocean Remote Sensing Conference (PORSEC). Kochi, Kerala, India, p 20.

McCreary JP, Murtugudde R, Vialard J, Vinayachandran PN, Wiggert JD, Hood RR, Shankar D, Shetye S (2009) Biophysical processes in the Indian Ocean. In: Wiggert JD, Hood RR, Naqvi SWA, Brink KH, Smith SL (eds) Indian Ocean biogeochemical processes and ecological variability. Geophys Monogr Ser 185:9–32. American Geophysical Union. https://doi.org/10.1029/2008GM000768

Moore SK, Trainer VL, Mantua NJ, Parker MS, Laws EA, Backer LC, Fleming LE (2008) Impacts of climate variability and future climate change on harmful algal blooms and human health. Environ Health 7:S4. https://doi.org/10.1186/1476-069X-7-S2-S4

Morrison JM, Codispoti LA, Gaurin S, Jones B, Manghnani V, Zheng Z (1998) Seasonal variation of hydrographic and nutrient fields during the US JGOFS Arabian Sea Process Study. Deep-Sea Res. II: Top Stud Oceanogr 45:2053–2101. https://doi.org/10.1016/S0967-0645(98)00063-0

Naqvi SWA, Jayakumar DA, Narvekar PV, Naik H, Sarma VVSS, D'Souza W, Joseph S, George MD (2000) Increased marine production of N2O due to intensifying anoxia on the Indian continental shelf. Nature 408:346–349. https://doi.org/10.1038/35042551

Nayak AR, Kolluru S, Kumar A, Bhadury P (2025) Revisiting harmful algal blooms in India through a global lens: an integrated framework for enhanced research and monitoring. iScience 28:111916. https://doi.org/10.1016/j.isci.2025.111916

O'Reilly JE, Maritorena S, Mitchell BG, Siegel DA, Carder KL, Garver SA, Kahru M, McClain C (1998) Ocean color chlorophyll algorithms for SeaWiFS. J Geophys Res Oceans 103:24937–24953. https://doi.org/10.1029/98JC02160

Padmakumar KB, Menon NR, Sanjeevan VN (2012) Is occurrence of harmful algal blooms in the exclusive economic zone of India on the rise? Int J Oceanogr 2012:263946. https://doi.org/10.1155/2012/263946

Raj KD, Mathews G, Obura DO, Laju RL, Bharath MS, Kumar PD, Arasamuthu A, Kumar TA, Edward JP (2020) Low oxygen levels caused by *Noctiluca scintillans* bloom kills corals in Gulf of Mannar, India. Sci Rep 10:22133. https://doi.org/10.1038/s41598-020-79152-x

Reddy BB, Vijayan AK, Sudheesh V, Sherin CK, Roy R, Vishnu NN, Gupta GVM (2024) Nutrient stoichiometry drives the phytoplankton populations during the progression of upwelling along the eastern Arabian Sea. Prog Oceanogr 229:103347. https://doi.org/10.1016/j.pocean.2024.103347

Retnamma J, Chinnadurai K, Loganathan J, Nagarathinam A, Singaram P, Jose AK (2021) Ecological responses of autotrophic microplankton to the eutrophication of the coastal upwelling along the Southwest coast of India. Environ Sci Pollut Res 28:11401–11414. https://doi.org/10.1007/s11356-020-11354-2

Roxy MK, Modi A, Murtugudde R, Valsala V, Panickal S, Prasanna Kumar S, Ravichandran M, Vichi M, Lévy M (2016) A reduction in marine primary productivity driven by rapid warming over the tropical Indian Ocean. Geophys Res Lett 43:826–833. https://doi.org/10.1002/2015GL066979

Sahay A, Ali SM, Gupta A, Goes JI (2017) Ocean color satellite determinations of phytoplankton size class in the Arabian Sea during the winter monsoon. Remote Sens Environ 198:286–296. https://doi.org/10.1016/j.rse.2017.06.017

Sahayak S, Jyothibabu R, Jayalakshmi KJ, Habeebrehman H, Sabu P, Prabhakaran MP, Jasmine P, Shaiju P, Rejomon G, Thresiamma J, Nair KKC (2005) Red tide of *Noctiluca miliaris* off south of Thiruvananthapuram subsequent to the 'stench event' at the southern Kerala coast. Curr Sci 89:1472–1473

Samanta A, Baliarsingh SK, Lotliker AA, Joseph S, Nair TMB (2023) Satellite-based detection of *Noctiluca* bloom in the coastal waters of the south-eastern Arabian Sea: a case study implicating monitoring needs. Natl Acad Sci Lett 46:103–107. https://doi.org/10.1007/s40009-023-01205-2

Sarma VVSS, Patil JS, Shankar D, Anil AC (2019) Shallow convective mixing promotes massive *Noctiluca scintillans* bloom in the northeastern Arabian Sea. Mar Pollut Bull 138:428–436. https://doi.org/10.1016/j.marpolbul.2018.11.054

Sarma VVSS, Udaya Bhaskar TVS, Pavan Kumar J, Chakraborty K (2020) Potential mechanisms responsible for occurrence of core oxygen minimum zone in the north-eastern Arabian Sea. Deep Sea Res Part I Oceanogr Res Pap 165:103393. https://doi.org/10.1016/j.dsr.2020.103393

Sathish T, Kuttippurath J, Purushothaman A, Amal KS, Mohan R, John L, Thomas LC, Padmakumar KB (2023) Observed evidence for the impact of coastal currents on the recurrent *Noctiluca scintillans* blooms in the northwest Indian Ocean coast. Mar Pollut Bull 194:115426. https://doi.org/10.1016/j.marpolbul.2023.115426

Sathyendranath S, Watts L, Devred E, Platt T, Caverhill C, Maass H (2004) Discrimination of diatoms from other phytoplankton using ocean-colour data. Mar Ecol Prog Ser 272:59–68. https://doi.org/10.3354/meps272059

Sathyendranath S, Stuart V, Nair A, Oka K, Nakane T, Bouman H, Forget MH, Maass H, Platt T (2009) Carbon-to-chlorophyll ratio and growth rate of phytoplankton in the sea. Mar Ecol Prog Ser 383:73–84. https://doi.org/10.3354/meps07998

Schott FA, McCreary JP (2001) The monsoon circulation of the Indian Ocean. Prog Oceanogr 51:1–123. https://doi.org/10.1016/S0079-6611(01)00083-0

Shahimol SR, Kalita R, Lotliker AA (2025) Application of satellite and bio-Argo float-based estimation of particulate organic carbon for ecosystem monitoring in the Arabian Sea. Mar Environ Res 212:107568. https://doi.org/10.1016/j.marenvres.2025.107568

Shetye S, Pratihary A, Shenoy D, Kurian S, Gauns M, Uskaikar H, Naik B, Nandakumar K, Borker S (2023) Rice husk as a potential source of silicate to oceanic phytoplankton. Sci Total Environ 879:162941. https://doi.org/10.1016/j.scitotenv.2023.162941

Shunmugapandi R, Gedam S, Inamdar AB (2024) Impact of 2015–2016 El Niño on phytoplankton size class distribution during the summer and winter monsoon in the Arabian Sea. Int J Remote Sens 45:9017–9032. https://doi.org/10.1080/01431161.2023.2295839

Sieburth JM, Smetacek V, Lenz J (1978) Pelagic ecosystem structure: heterotrophic compartments of the plankton and their relationship to plankton size fractions. Limnol Oceanogr 23:1256–1263. https://doi.org/10.4319/lo.1978.23.6.1256

Smetacek V (1999) Diatoms and the ocean carbon cycle. Protist 150:25–32. https://doi.org/10.1016/S1434-4610(99)70006-4

Stoecker DK, Hansen PJ, Caron DA, Mitra A (2017) Mixotrophy in the marine plankton. Annu Rev Mar Sci 9:311–335. https://doi.org/10.1146/annurev-marine-010816-060617

Stramski D, Reynolds RA, Babin M, Kaczmarek S, Lewis MR, Röttgers R, Sciandra A, Stramska M, Twardowski MS, Franz BA, Claustre H (2008) Relationships between the surface concentration of particulate organic carbon and optical properties in the

eastern South Pacific and eastern Atlantic Oceans. Biogeosciences 5:171–201. https://doi.org/10.5194/bg-5-171-2008

Sweeney BM (1971) Laboratory studies of a green *Noctiluca* from New Guinea. J Phycol 7:53–58. https://doi.org/10.1111/j.1529-8817.1971.tb01478.x

Tarran GA, Burkill PH, Edwards ES, Woodward EMS (1999) Phytoplankton community structure in the Arabian Sea during and after the SW monsoon, 1994. Deep Sea Res Part II Top Stud Oceanogr 46:655–676. https://doi.org/10.1016/S0967-0645(98)00122-2

Thoppil PG (2023) Enhanced phytoplankton bloom triggered by atmospheric high-pressure systems over the Northern Arabian Sea. Sci Rep 13:769. https://doi.org/10.1038/s41598-023-27785-z

Tréguer P, Bowler C, Moriceau B, Dutkiewicz S, Gehlen M, Aumont O, Bittner L, Dugdale R, Finkel Z, Iudicone D, Jahn O, Guidi L, Lasbleiz M, Leblanc K, Levy M, Pondaven P (2018) Influence of diatom diversity on the ocean biological carbon pump. Nat Geosci 11:27–37. https://doi.org/10.1038/s41561-017-0028-x

Uitz J, Claustre H, Morel A, Hooker SB (2006) Vertical distribution of phytoplankton communities in open ocean: an assessment based on surface chlorophyll. J Geophys Res Oceans 111:C08005. https://doi.org/10.1029/2005JC003207

Wiggert JD, Hood RR, Banse K, Kindle JC (2005) Monsoon-driven biogeochemical processes in the Arabian Sea. Prog Oceanogr 65:176–213. https://doi.org/10.1016/j.pocean.2005.03.008

Xiang C, Tan Y, Zhang H, Liu J, Ke Z, Li G (2019) The key to dinoflagellate (*Noctiluca scintillans*) blooming and outcompeting diatoms in winter off Pakistan, northern Arabian Sea. Sci Total Environ 694:133396. https://doi.org/10.1016/j.scitotenv.2019.07.202

Zahir M, Balaji-Prasath B, Su YP, Feng S, Zou J, Yang Y (2023) The dynamics of red *Noctiluca scintillans* in the coastal aquaculture areas of Southeast China. Environ Geochem Health 45:4995–5012. https://doi.org/10.1007/s10653-023-01528-5

Publisher's note Springer Nature remains neutral with regard to jurisdictional claims in published maps and institutional affiliations.

Springer Nature or its licensor (e.g. a society or other partner) holds exclusive rights to this article under a publishing agreement with the author(s) or other rightsholder(s); author self-archiving of the accepted manuscript version of this article is solely governed by the terms of such publishing agreement and applicable law.